Synthesis and Characterization of the Properties of

Ti$_3$SiC$_2$/SiC and Ti$_3$SiC$_2$/TiC Composites

A Thesis

Submitted to the Faculty

of

Drexel University

by

Linh H. Ho-Duc

in partial fulfillment of the

requirements for the degree

of

Master of Science

in

Materials Engineering

January 2002

DEDICATIONS

To my parents and Nuong Bui, for their unconditional support.

ACKNOWLEDGEMENTS

TABLE OF CONTENTS

LIST OF TABLES

LIST OF FIGURES

Abstract
Synthesis and Characterization of Properties of
Ti_3SiC_2/SiC and Ti_3SiC_2/TiC Composites
Linh H. Ho-Duc
Michel W. Barsoum and Tamer El-Raghy

In 1996, the ternary compound titanium silicon carbide (Ti_3SiC_2) was for the first time

synthesized as a single-phase, fully dense compound. Its characterization revealed a

unique combination of properties. For its high fracture toughness, low hardness to

elastic modulus ratio and excellent damage tolerance, it was dubbed a soft ceramic. It

also displayed good thermal shock and oxidation resistance. In this work, the

reinforcement of this material with silicon carbide and titanium carbide particles was

explored with the intention of improving mechanical and oxidation properties. The

composites were synthesized by HIPing of starting powders, following the same

processing as for pure Ti_3SiC_2.It was found that the particles affected the microstructure

of the Ti_3SiC_2 matrix, reducing the grain size of a material that otherwise would have

been coarse-grained. Mechanical properties of the composites were investigated through

four-point bend tests and Vickers indentations. The flexural strength of the composites

was lower than expected from the grain size of the matrix and was explained by a

thermal expansion coefficient mismatch. Fracture toughness of the composites was also

lower than for Ti_3SiC_2. However, the hardness and damage tolerance were improved.

Oxidation experiments were conducted in air at temperatures ranging between 875°C

and 1220°C. The oxidation behavior of the Ti_3SiC_2/SiC composite was found to be

subparabolic at 925°C, but from 1010°C to 1220°C, it was parabolic with a transition to

linear behavior. The oxidation of the Ti_3SiC_2/TiC composite was parabolic at 875°C, and

from 975°C to 1220°C, showed the same behavior as the other composite. The growth of

the oxide scale of the composites was fitted with a multiple-law model. It was determined that the oxidation of the composites occurred by diffusion of oxygen inward and titanium outward. The parabolic component of the oxide scale growth was found to correspond to the diffusion of oxygen inward, as in pure Ti_3SiC_2. The corresponding parabolic constants were found to be lower for Ti_3SiC_2/SiC and higher for Ti_3SiC_2/TiC, compared to the pure material.

I SYNTHESIS AND CHARACTERIZATION OF TI$_3$SIC$_2$/SIC AND TI$_3$SIC$_2$/TIC COMPOSITES

A. <u>Background</u>

Jeitschko and Nowotny first discovered titanium silicon carbide in 1967[1]. They had been synthesizing a large number of carbides and nitrides in the 60's, when they discovered a series of phases now called Hägg phases. These phases have a chemistry of the form M_2AX, where M is an early transition metal, A is an A-group element (usually IIIA and IVA) and X is either C and/or N. Their unit cell is hexagonal and they are made of layers of M_2X separated by layers of pure A. It is in this context that Ti_3SiC_2 was discovered. It was related to the Hägg phases through its unit cell, which was made of layers of TiC_x between pure layers of Si. Figure 1 shows the unit cell of Ti_3SiC_2. The only other two phases of the same chemistry are Ti_3GeC_2 and Ti_3AlC_2. The former[2] was discovered at the same time as Ti_3SiC_2, while the latter[3, 4] was found in the 90's. Table 1 presents all the related phases that have been discovered up to date.

In 1967, Jeitschko and Nowotny were not able to characterize the mechanical properties of Ti_3SiC_2 for lack of a means to synthesize a phase pure and dense compound. In 1972, Nickl, Schweitzer and Luxenberg synthesized it by chemical vapor deposition (CVD) and reported an anomalously low hardness for a ceramic[5].

In spite of this troubling fact, interest in Ti_3SiC_2 was lost for nearly two decades, until Goto and Hirai confirmed the results obtained by Nickl *et al.* in 1987[6]. Others then

followed suit with more studies on CVD Ti_3SiC_2[7-9]. However, CVD has the particular disadvantage of having slow deposition rates. This is fine for crystal structure measurements and maybe microhardness measurements, but is not viable for characterization of other properties. A more practical and less time-consuming method for synthesis of bulk pieces of Ti_3SiC_2 was needed.

Over the years, there have been several attempts at fabricating bulk dense and single-phase samples of Ti_3SiC_2. They were successful to a certain degree, but were plagued by the sizeable presence of TiC or SiC as impurity.

The first to try were Pampuch and Lis[10-15], using self-propagating high-temperature synthesis (SHS) of powders of Ti, Si and carbon black. The resulting powders were pressureless sintered or hot pressed to obtain the final product, which contained about 20 vol% TiC. They also used hot isostatic pressing combined with SHS in different fashions, but obtained no better results in terms of purity of the Ti_3SiC_2[14].

Racault and Langlais[16] also synthesized Ti_3SiC_2 using a solid-state three-step processing route. It consisted in removing unwanted phases through chemical reactions and oxidation. It yielded about 5 mol% TiC as an impurity. Others also tried[17, 18], and all obtained TiC, SiC or both as impurity, usually at least a few percents.

Finally, in 1996, El-Raghy and Barsoum managed to synthesize a sample of Ti_3SiC_2 with less than 1% impurity by using Hot Isostatic Pressing (HIP)[19]. Since then, there have been many other papers devoted to the synthesis of nearly pure Ti_3SiC_2[20-26].

Only a few authors have reported on the fabrication of composites with a Ti_3SiC_2 matrix. Although many of the papers were technically dealing with Ti_3SiC_2/TiC composites,

none have recognized it as such, since their goal was to synthesize pure Ti_3SiC_2. Only Tong *et al.*[27] and Radhakrishnan *et al.*[28] have synthesized Ti_3SiC_2/SiC composites and studied their properties.

Tong *et al.*[27] synthesized a composite with 20 vol% SiC and 8 vol% TiC by hot pressing Ti_3SiC_2 and β-SiC powders at 1600°C. They reported that the presence of fine SiC particles limited the grain growth of Ti_3SiC_2. It also enhanced its Vickers hardness, fracture toughness, flexure strength at temperatures up to 1200°C, as well as its oxidation resistance.

Radhakrishnan *et al.*[28] used a displacement reaction between TiC and Si. They vacuum hot pressed the powders to obtain a composite consisting of Ti_3SiC_2 with about 14 vol% finely dispersed SiC as reinforcing phase and traces of $TiSi_2$. The SiC phase was found in 2 distinct shapes, namely, fine needles and blocks, and was also found to increase hardness and fracture toughness compared to monolithic Ti_3SiC_2.

B. Synthesis

Two composites were synthesized with the following target compositions:

- 70 vol% Ti_3SiC_2 / 30 vol% SiC, and

- 70 vol% Ti_3SiC_2 / 30 vol% TiC.

For each composition, two samples were made, with different processing parameters. The first batch of samples, comprising one sample of each composition, was Hot

Isostatically Pressed (HIPed) at a temperature of 1600°C for 8 hours, whereas the second batch was HIPed at 1500°C for 8 hours. For ease of reference, the samples will be named S1600 and S1500 for the samples containing silicon carbide processed at 1600°C and 1500°C, respectively. Similarly, the samples containing TiC will be referred to as T1600 and T1500.

The S1600 and T1600 samples were obtained by mixing titanium dihydride (TiH_2), α-silicon carbide (SiC, -400 mesh, particle size distribution shown in Figure 2) and graphite (C) in their respective stoichiometric quantities. These mixtures were dry ball-milled for about 1 hour and cold isostatically pressed (CIPed) at a pressure of 350 MPa. The green bodies were heated under vacuum at 900°C for 6 hours in order to dehydride the mixtures. The resulting green bodies were HIPed at 1600°C for 8 hours under a pressure of ~200 MPa to obtain the samples that were tested.

For sample S1500, powders of titanium (Ti), α-SiC (fine, 0.1-5 μm) and C were mixed in stoichiometric quantities to form the composite. Figure 3 shows the particle size distribution of the SiC powder, as measured in a laser scattering particle size analyzer (Horiba LA-910). The mixture was ball-milled for one hour then held at 200⁰C in a vacuum furnace for 2 hours to get rid of moisture. The mixture was dry ball-milled again for 15 minutes in order to break agglomerates and tapped into glass cylinders. The cylinders were placed in a vacuum furnace and heated to a temperature of 600⁰C in vacuum for 2 hours. The tubes were finally vacuum sealed and placed in a hot isostatic press, where they were heated at a temperature of 1500⁰C for a total of 8 hours under a pressure of ~200 MPa to obtain the final sample.

Sample T1500 underwent the same processing as S1500 but the starting powders were Ti, SiC and C in stoichiometric quantities to form Ti_3SiC_2, with an addition of TiC powder sufficient to form a volume fraction of 30% in the composite.

After synthesis, a cross-section of each sample was cut, mounted and polished using SiC grinding paper followed by diamond solutions down to 1 μm. The polished surface was etched with a 1:1:1 by volume solution of water, HF and HNO_3. The etched surfaces were observed under an optical microscope (Olympus, PMG-3). Porosity, SiC and TiC volume fractions were determined by area fraction measurements.

The polished and unetched surface of Ti_3SiC_2 appears white under the optical microscope. SiC and pores appear grey and black, respectively, while TiC appears white, even after overetching. Using a black and white camera that captures images from the microscope and digitizes them, it is possible to adjust the image such that the desired phase to be measured is contrasted with respect to the background. A software is then used to compute the area fraction of the image that is white or black. Using this method before etching to measure porosity and SiC content (as black phases), and after overetching to measure TiC content (as white phases), it is possible to measure the area fractions of the different phases.

Particle size of the reinforcing phases was measured using the linear intercept method. For Ti_3SiC_2, the length of each grain crossing a random line was measured.

Density of the samples was measured using the Archimedean method.

C. <u>Characterization</u>

All samples processed were dense, with a small measured amount (< 2%) of closed porosity.

Figure 4 shows the polished and etched surface of S1600. By surface fraction measurement, the volume fraction of SiC was found to be approximately 30% and that of TiC 4%. The SiC phase was dispersed throughout the matrix. Figure 5 shows the particle size distribution of the reinforcing particles in all four composites. As can be seen, the grain size of the SiC particles in S1600 varied from a few microns to ~50 μm. Figure 6 shows the grain size distribution of the Ti_3SiC_2 matrix in the composites. The Ti_3SiC_2 matrix of S1600 presented a rather fine-grained structure, with many small grains of the order of 1 to 20 μm and few larger grains that could grow up to 70 μm. However, grains larger than 40 μm accounted for 50% of the volume.

Figure 7 represents the microstructure of T1600. From surface area measurements, the TiC volume fraction was 30% and that of SiC was 3%. The grain size of the matrix was more uniform than in S1600, with an average of 10 μm (Figure 6), but the TiC phase was made of smaller agglomerated grains partially sintered together. This gave a "network" shape to the TiC grains in the matrix, which is why the microstructure appeared non-homogeneous. The average grain was about 10 μm, and any grain larger than that should be considered an agglomerate (Figure 5). One way to ascertain this is to use Orientation Imaging Microscopy (OIM) in order to distinguish neighboring grains from each other by their crystal orientation.

Figure 8 shows the microstructure of S1500. The volume fraction of SiC was about 30% and for TiC, about 3%. The grain size of SiC particles varied from 1 to 40 μm (Figure 5), but the starting powder being very fine (see Figure 3), it is reasonable to assume that grain growth occurred. Furthermore, the disposition of the SiC grains seemed to be similar to that observed for TiC in T1600, the only difference being that SiC grains grew whereas the TiC grains sintered. For the matrix, the grain size was mostly fine with some larger grains, as in S1600, but there were less of them (Figure 6). Also, the size distribution of the smaller grains was narrower than in S1600.

Figure 9 shows the microstructure of T1500. The volume fraction of TiC was about 29%, with a volume fraction of SiC less than 1%. Here, at the difference of sample T1600, the TiC grains were less agglomerated and agglomerates were at most 20 μm large, but most were not sintered and were about 5 μm large. The matrix was similar to T1600 and the grain size was uniform, with an average of 10 μm. The difference between the two Ti_3SiC_2/TiC composites, other than the processing temperature, may come from the difference in starting powders.

T1500 was mixed starting with 30 vol% TiC powder, whereas T1600 started with TiH_2 and C to form TiC. Since TiC had to be formed by reaction between titanium and carbon, it is probable that the nucleation of TiC grains was heterogeneous, and that nucleation sites were not equally distributed throughout the material. This would have lead to regions of high TiC concentration. As Ti_3SiC_2 formed from $Ti_5Si_3C_x$ and TiC_x, regions containing almost exclusively TiC did not react for lack of $Ti_5Si_3C_x$. This could explain the "network" structure of TiC in T1600. In contradistinction, since T1500 started with

pre-existing TiC, it was well dispersed after ball milling and remained that way during processing.

Table 2 shows the measured densities of the samples along with their theoretical densities, taking into account the volume fractions of all secondary phases. The calculated relative densities, with a minimum of 97%, agree with the measured porosity of the samples.

D. Effect of Reinforcing Phases on Grain Size of Ti_3SiC_2 Matrix

In previous work, El-Raghy and Barsoum[29] constructed a map of the microstructures obtained under different processing temperatures and times in the HIP. According to this map, the evolution of the microstructure starts with a fine-grained microstructure (grain size: ~ 5-10 μm), which is followed by a duplex microstructure when some of the grains grow abnormally large compared to the rest (100-200 μm), to end up in a coarse microstructure, where most grains have grown to a large size. The data in this map shows that HIPing Ti_3SiC_2 at 1600°C for 8 hours would result in a coarse-grained microstructure, whereas HIPing Ti_3SiC_2 at 1500°C for 8 hours would yield a duplex microstructure. Comparing with the results obtained in this work, it is obvious that the presence of TiC and SiC as secondary phases has an effect on the microstructure of the matrix.

In the case of TiC, the microstructure has remained relatively fine-grained, with a grain size of about 10 μm as opposed to the few hundred microns of the coarse-grained

Ti_3SiC_2, at either processing temperature. This confirms the assumption that TiC inhibits the grain growth of Ti_3SiC_2, or, rather, TiC inhibits the exaggerated grain growth observed in Ti_3SiC_2 by pinning grain boundaries, and does not allow the grains to grow much larger than 20 μm.

The effect of SiC seems to be a little more subtle, since we still observe some abnormal grain growth (shown in Figure 10), although the size of the large grains is not as exaggerated as in pure Ti_3SiC_2, reaching only about 70 μm at both temperatures. However, there were more abnormal grains at 1600°C than at 1500°C. Although there is an impeding effect from SiC, it is not as pronounced as with TiC.

The difference between TiC and SiC in terms of the structures they form within the Ti_3SiC_2 matrix is that the TiC grains sintered together, as can be attested by the shape of the large particles, which still show evidence of a neck between sintered particles, whereas SiC grains grew, as shown by the hexagonal corners of the large grains. There was also some sintering among adjacent SiC grains, but to a much lesser extent than for TiC. This means that SiC has to have some solubility in Ti_3SiC_2 in order to diffuse and allow the SiC grains to grow, unless grain growth occurred only when some SiC grains were adjacent to each other. However, this last part is unlikely, since there should be much more grain growth, and much less small grains that did not grow or disappear as a result of coarsening, unless there were other factors affecting the growth of SiC grains. Since this coarsening behavior is not seen in TiC particles, there is no evidence that TiC is soluble in Ti_3SiC_2. There is also no evidence that TiC is not soluble in Ti_3SiC_2.

Another possible source of SiC for grain coarsening would be the matrix itself. If SiC were to be leeched out of the matrix in order for the SiC grains to grow, there would be traces of TiC_x and probably Ti metal around the grown SiC grains, since SiC removed from the matrix would leave 3 Ti atoms and one C atom. This was not observed in the microstructure, so this possibility is not viable.

There is one mechanism through which there would be no need for solubility of SiC in Ti_3SiC_2. The Nash-Higgins model[30] is a model in which the dispersed particles are dragged by the moving grain boundaries of the matrix, causing them to agglomerate at grain boundaries and come into contact with each other. When contact is established, SiC can directly diffuse from a smaller particle to a larger one without having to pass through Ti_3SiC_2. Although there is no confirmation that this mechanism is operative, it is an interesting avenue to explore in understanding the grain growth mechanism of SiC in Ti_3SiC_2. Much work would also be needed to distinguish between this model and diffusion of SiC through Ti_3SiC_2, a prospect that lies beyond the scope of this work.

As can be inferred from the previous discussion, there is much ground for speculation here, because the focus in this synthesis was not on studying the grain growth of SiC particles within the matrix. Therefore, other crucial data, such as microstructural characteristics at shorter and longer processing times were left out. All that can be said in certainty is that SiC has to diffuse somehow in order to have grain growth. It is not known at this time what the mode of diffusion is, or what its path is. The only two other studies of Ti_3SiC_2/SiC composites[27, 28] did not encounter such issues, because their processing times were much shorter. The size of SiC particles in their composites did not

exceed 5 μm. Radhakrishnan *et al.* reported two different shapes, namely needles and blocks, whereas Tong *et al.* showed only blocks in their composites.

The coarsening of SiC grains could be used to explain the difference in microstructure observed between S1600 and S1500. Comparing Figures 6 and 8, which are at the same approximate scale, it can be seen that the SiC particles in S1600 are all quite coarse, whereas in S1500, they are of smaller size and more numerous. This difference comes not only from the coarsening of SiC grains, but also from the fact that the starting SiC powders in S1600 were coarser than in S1500. This difference in size distribution, which then relates to a difference in number density of particles, can translate into a smaller mean free path between SiC particles within the matrix in S1500. This, coupled with the lower grain growth kinetics of the matrix at lower temperature, is what probably contributed to the difference in the microstructure of the matrix in S1600 and S1500.

E. Conclusions

The composites Ti_3SiC_2/SiC and Ti_3SiC_2/TiC containing 30 vol% of the reinforcing phase and less than 4 vol% impurities were synthesized by hot isostatic pressing. TiC was confirmed to be effective in reducing the grain size of the matrix to a maximum of about 20 μm, no matter how disperse the phase was. SiC proved to be less effective in controlling the matrix grain size, due to its coarsening behavior in the matrix, leading to some abnormal grain growth. The coarsening behavior of SiC led to the belief that it may be able to diffuse through Ti_3SiC_2, although the mode of diffusion and diffusion path are open to speculation.

II MECHANICAL PROPERTIES

A. <u>Background</u>

Apart from its hardness, nothing was known of the mechanical properties of pure Ti_3SiC_2 before El-Raghy and Barsoum investigated them. Nickl *et al.*[5] reported a hardness corresponding to ~12 to 15 GPa (Vickers hardness) in a direction normal to the basal planes and ~3 to 4 GPa in directions parallel to the basal planes on CVD Ti_3SiC_2. Goto and Hirai confirmed that result in their work, with an asymptotic value for hardness of about 6 GPa at a load of 1 kg, as the average of a polycrystalline material with randomly oriented grains. Lis and Pampuch reported a Young's modulus of 326 GPa and shear modulus of 135 GPa[11] on Ti_3SiC_2 containing 10-20 vol% TiC. Okano *et al.*[17] reported a flexural strength of 560 MPa at room temperature and a fracture toughness of 6.9 MPa-m$^{1/2}$ using a single edge pre-cracked beam (SEPB) method, on Ti_3SiC_2 that was 95% dense and contained a few percents of impurities.

El-Raghy and Barsoum[31-35] reported on the mechanical properties of Ti_3SiC_2 for two distinct microstructures: a fine-grained (FG) microstructure, with grains 3 to 5 μm in size, and a coarse-grained (CG) microstructure, with grains 100 to 200 μm in size. The elastic modulus was determined to be ~320 GPa. The flexural strength of Ti_3SiC_2 at room temperature was found to be approximately 600 MPa and 320 MPa for FG and CG microstructure, respectively. It was found to decrease sharply above 1100°C. The hardness was found to decrease with increasing load to reach an asymptotic value of 4 GPa in both microstructures. This result confirmed the prediction by Pampuch and co-

workers[14] from measurements of the hardness of polycrystalline Ti_3SiC_2 with different TiC contents. CG Ti_3SiC_2 was found to be damage tolerant with Vickers indentation loads up to 10 N, as well as thermal shock resistant. FG Ti_3SiC_2 was found to be damage tolerant up to 10 N and susceptible to thermal shocks between 750 and 1000°C.

The fracture toughness was initially reported as being ~ 6 MPa·$m^{1/2}$ using single edge notched beams[32] (SENB). More recently, however, values of 9.5 MPa·$m^{1/2}$ for the FG microstructure and 14 to 16 MPa·$m^{1/2}$ for the CG microstructure were derived from rising resistance-curve behavior[35, 36]. The latter are very high values compared to any conventional ceramic.

Li *et al.*[37] also measured the fracture toughness of a sample containing about 3 vol% TiC with a duplex microstructure, containing few coarse grains (100-200 μm in length) surrounded by smaller grains. They used a SENB method and measured the fracture toughness at room temperature to be 4.52 ± 0.15 MPa·$m^{1/2}$, which is very low compared to the value found by El-Raghy. The obvious discrepancy between results seems to be related to the difference in the method used to measure fracture toughness.

For composite materials, Tong *et al.*[27] measured the flexural strength, fracture toughness and Vickers hardness of Ti_3SiC_2/SiC with 20 vol% SiC and 8 vol% TiC. The flexural strength at room temperature was higher than what they had measured previously[17] in monolithic Ti_3SiC_2, with a small improvement from 560 MPa to about 600 MPa. The improvement was much greater at 1200°C, attributed to the restriction of plastic deformation in the composite. The fracture toughness, measured by single edge pre-cracked beam (SEPB), was 5.4 MPa·$m^{1/2}$, a lower value than previously measured for the

monolithic body. This was attributed to a lack of large grains to deflect cracks. Finally, the Vickers hardness was measured to be 10.6 GPa under a load of 98N.

Radhakrishnan *et al.*[28] also measured Vickers hardness and fracture toughness on their composite, which contained 14 vol% finely dispersed SiC. They found the hardness to be 8.9 ± 0.3 GPa and to be constant at loads from 9.8 to 98 N. This value is consistent with the results obtained by Tong *et al* if it is assumed that the increased hardness compared to monolithic Ti_3SiC_2 is due to the presence of SiC. The samples of Tong *et al.* contained more SiC, as well as more TiC, which is even harder, and therefore should show higher hardness. However, no quantitative relationship between reinforcing phase content and hardness can yet be established without more data. The fracture toughness of the composite was calculated from Vickers indents that showed crack development, and was found to be 9.1 ± 0.6 MPa-$m^{1/2}$. Since this is the only work that ever measured fracture toughness using Vickers indentations, there is no basis for comparison.

B. Experimental Details

Mechanical properties of the Ti_3SiC_2/SiC and Ti_3SiC_2/TiC composites were investigated using a Vickers indenter (American Machine and Metals, Riehle, East Moline, IL) and a stainless steel 4-point bend testing apparatus shown in Figure 11, with relevant dimensions.

The samples for 4-point bend tests were machined using an Electric Discharge Machine (EDM) to the dimensions of 1.5 x 2 x 25 mm, in accordance with ASTM C1161 Type A[38].

After machining, the tensile surfaces were lightly ground by hand on grit 1200 silicon carbide grinding paper. Any part of the apparatus in contact with the sample was dipped in oil to minimize the effects of friction. The experimental apparatus was placed in a testing machine in compression mode (MTS) and the crosshead speed was set to 0.1 mm/s. Upon breaking of the sample, the peak load was recorded and the point at which the break occurred was checked to validate the test.

The flexural strength of the sample was determined using the following equation:

$$\sigma = \frac{3\,P\left(l_1 - l_2\right)}{2\,B\,H^2} \times 1000 \tag{1}$$

where σ is the flexural strength in MPa, P is the peak load in N, l_1 is the outer span and l_2 the inner span in mm, B is the width of the cross-section of the sample and H is its height in mm. Refer to Figure 11 for actual dimensions.

Aside from measuring the flexural strength of the samples, damage tolerance and thermal shock resistance were also measured. Damage tolerance was measured by first indenting the tensile side of the 4-point bend samples with a Vickers indenter, using loads of 10, 20, 30 or 50 kg. After the indentation, the sample was tested in four-point bend, following the procedure outlined above. The measured flexural strength of the sample after indentation is called the retained flexural strength of the sample.

Thermal shock was performed by heating an alumina tube furnace in air to the desired temperature, then introducing the samples in the furnace. The sample was held at temperature for 15 minutes, before being rapidly dropped into a bucket of water at room

temperature. The initial temperatures used were 700, 1000, 1200 and 1400°C. After thermal shock, the retained flexural strength of the samples was also measured.

For each load and each temperature, five samples were used. The retained flexural strength was measured in each case using the same parameters as described above.

For Vickers hardness measurements, samples were cut to have a large enough cross-section and were mounted. The mounted samples were ground with silicon carbide grinding paper up to 1200 grit and polished with diamond suspensions of 3 µm and 1 µm. Indentations were made on the polished surface. For S1600, T1600 and S1500, at least 10 indentations were made for each load of 10, 20 and 30 kg. In addition, another 12 indentations were made using a 50 kg load on S1500 and T1600. The indentation diagonal was measured in the SEM and the Vickers hardness was obtained through the use of the following equation:

$$\text{VHN (GPa)} = \frac{18187.74 \times \text{P}}{a^2} \tag{2}$$

P is the indenter load in kg and a is the indentation diagonal in µm. T1500 was not tested because of the belief that its mechanical properties were not significantly altered using a lower HIPing temperature. This will be explained in a later section of this chapter.

Among the indentations made on the samples, only one indentation showed cracks on S1500 under a load of 30 kg (Figure 12). On T1600, 3 indentations developed cracks (Figure 13 shows one). From these cracks, an estimate of the fracture toughness of the composite was calculated using an expression from Evans and Charles[39]:

$$K_{ic}\left(MPa - m^{1/2}\right) = \left(\frac{H}{3E}\right)^{0.4} \times H \times \sqrt{a} \times \left(\frac{c}{a}\right)^{-3/2} \tag{3}$$

where H is the Vickers hardness at the load used for the indentation, in MPa; E is

Young's modulus, in MPa; a is half the indentation diagonal and c is the distance from

the center of the indentation to the extremity of the crack, in meters.

Another expression developed by Anstis *et al.*[40] was also used:

$$K_{ic}\left(MPa - m^{1/2}\right) = 0.016\left(\frac{E}{H}\right)^{1/2} \times \left(\frac{P}{c^{3/2}}\right) \times 10^{-6} \tag{4}$$

where E, H and c have the same meaning as in Equation (3), and P is the indentation

load in N.

The stiffness of the composites was estimated using a simple rule of mixture, to estimate

their specific modulus.

C. <u>Results and Discussion</u>

Flexural Strength

Table 3 summarizes flexural strength for all samples, and shows thermal shock

resistance and damage tolerance data in the most extreme conditions for comparison

between samples.

As can be seen in Table 3, the lower processing temperature resulted in an increase in flexural strength of almost 50% for the Ti_3SiC_2/SiC composite. There was also an improvement on damage tolerance and thermal shock resistance by about 25%, but it will be shown later that this improvement is not general.

In contrast, for the Ti_3SiC_2/TiC composite, there was not much change in the flexural strength, except for a larger standard deviation. Because there was no significant change in flexural strength, the thermal shock resistance, damage tolerance and hardness of T1500 were not measured. Indeed, assuming that the behavior of the two composites is similar, one can infer that the increase in damage tolerance and thermal shock resistance would not be significant for the Ti_3SiC_2/TiC composite.

The flexural strength reported by El-Raghy and Barsoum for monolithic Ti_3SiC_2 was ~600 MPa for fine-grained material and ~ 300 MPa for coarse-grained material. Obviously, although the microstructure of the matrix was closer to a fine-grained microstructure than to a coarse-grained one, the flexural strength of the composites is lower than for comparable grain sizes of the monolithic material. This can be explained if the difference in thermal expansion coefficients of the materials is taken into account.

The thermal expansion coefficients of SiC, TiC and Ti_3SiC_2 are, respectively, 5.12×10^{-6}/K[41], 7.4×10^{-6}/K[41], 8.6×10^{-6}/K (Ti_3SiC_2, a-direction) and 9.7×10^{-6}/K (Ti_3SiC_2, c-direction)[34]. Since the reaction and sintering of the microstructure happens at 1600°C, it is assumed that at 1600°C, all grains are strain-free.

When the sample cools down, there is a thermal expansion mismatch between reinforcing particles and the matrix, with the matrix shrinking faster than the particles.

This results in residual strains, which lead to the reinforcing particles being put under a compressive stress, and the matrix region around them experiencing a hoop tensile stress. This pre-existing stress concentration around reinforcing particles weakens the microstructure and could explain the loss of flexural strength of the composites compared to the monolithic material.

Since the thermal expansion of TiC is closer to that of Ti_3SiC_2, it follows that the thermal expansion mismatch is less severe in the case of TiC, and this would result in the higher flexural strength for the Ti_3SiC_2/TiC composite, compared to the Ti_3SiC_2/SiC composite. In addition, the size of the reinforcing particles also plays a role in the flexural strength of the composites. As the reinforcing particles size increases, or the size of their agglomerates, so does the strain mismatch around them, which offers an explanation for the difference in strength between S1500 and S1600. This same factor also accounts for the better strength of T1600, since its TiC average grain size is smaller than the SiC average grain size for any of the Ti_3SiC_2/SiC composites.

In addition to thermal expansion mismatch effects, there is one other factor that could lead to an overestimate of those effects. It has been established that the flexural strength of Ti_3SiC_2 is controlled by its grain size, which is the source of its defects[33]. As of now, no empirical law has been established, mainly because it is difficult, if not impossible, to synthesize phase pure Ti_3SiC_2 with intermediate grain sizes between the FG and CG microstructures, because of the abnormal grain growth phenomenon. However, it can safely be said that the flexural strength of Ti_3SiC_2 decreases as its grain size increases. Here, Figure 5 suggests that S1500 has the smallest and narrowest grain size distribution, which should put it above the rest in terms of strength, but it is not.

Therefore, the matrix grain size effect is not as important as the thermal expansion mismatch effect.

Damage Tolerance

Figure 14 shows complete data for the various damage tolerance tests, as well as results previously obtained on monolithic Ti_3SiC_2, for comparison. The strength of the composites is closer to that of coarse-grained titanium silicon carbide, even though their matrix grain sizes are closer to fine-grained Ti_3SiC_2.

Of the samples tested, T1600 and S1600 showed the best damage tolerance. They kept their original strength even after a Vickers indentation of 98 N. These indentations are about 100 μm in diagonal and 15 μm in depth, assuming no elastic recovery. At 490 N, the same dimensions were about 350 μm and 50 μm. In comparison, the retained strength of S1500 started decreasing right away. However, compared to S1600, it showed an improvement in retained strength over the whole range tested by at least 30%. Plotting the data on a log-log scale as in Figure 15 shows that the composites start transitioning between microstructure controlled fracture and indentation load controlled fracture[42] around 98 N. The fact that the slope between original strength and the 98 N point for S1500 is slightly negative suggests that the transition starts at a lower load for S1500, but probably close to 98 N. In comparison, alumina, barium titanate or glass-ceramics were shown to start transitioning at loads of a few Newtons at the most[42]. This makes a difference of two orders of magnitude!

Thermal Shock

Figure 16 plots the results of the thermal shock resistance tests (actual data values shown in Table 4), with previous results on monolithic Ti_3SiC_2 for comparison. Again, the thermal shock behavior of the composites was most similar to coarse-grained Ti_3SiC_2 with an expected dip in retained strength before increasing again.

Figure 16 shows that only S1600 retained its strength after a thermal shock from 700°C, since it started at an already low value. This means that the size of the flaws introduced in S1600 by the thermal shock was not greater than the original flaw size. The two other samples, after the same thermal shock, sank to the same strength, even though they started at a higher initial strength. Another point of somewhat lesser importance is that the minimum retained strength occurred at 1000°C both for S1600 and T1600, whereas S1500 experienced its minimum at 1200°C. Since these thermal shock experiments were done at large temperature intervals, it would be safer to say that the minima for retained strength occurred at temperatures near the indicated temperature.

It is possible that the slight increase in retained flexure strength of the samples was due to the formation of a thin oxide layer at the surface of the samples, because the samples were heated in air. At temperatures higher than 1000°C, 15 minutes would be enough to form a thin oxide layer. This oxide layer experiences compressive stresses due to its increase in volume compared to the original material. These compressive stresses could be enough to justify the increase in retained strength at high temperatures. Thermal

shock experiments where the samples are heated in flowing argon can be conducted to confirm this supposition.

Hardness

Figure 17 shows the results obtained from Vickers macrohardness measurements. The large standard deviations present especially at low loads can be explained by the lack of homogeneity of the microstructure at the size scale of the indents. Since the reinforcing phases are much harder than Ti_3SiC_2 (28-35 GPa for TiC[41] and 24-28 GPa for SiC[41]), if an indent were to be centered on a reinforcing particle or agglomerate, it would result in a smaller indentation size than it would be on Ti_3SiC_2, and a higher reading, increasing the scatter of the data. As the indentation load increases, the area affected by the indentation increases, and there is more chance for it to have a homogeneous response.

As indentation load increased, the hardness decreased for all samples. T1600 showed the highest hardness among the samples for the same indentation load, remaining at 15 GPa up to 196 N, then decreased to almost half its value at 294 N. The hardness then remained the same at 490 N, with an asymptotic value of 8.2 ± 0.9 GPa.

The hardness of S1600 and S1500 were different under a load of 98 N, but they reached almost identical values as the load increased to 294 N, even matching with a small increase in hardness from 196 to 294 N. This suggests that S1600 would have a very similar hardness to S1500 under a load of 490 N. It also suggests that the hardness at higher loads is not dependent on the microstructure of the matrix or reinforcing phase

anymore. Therefore, the asymptotic hardness value of S1600 and S1500 was found to be 6.9 ± 0.7 GPa.

Comparing the data obtained at 98 N with the results obtained by Tong *et al.*[27] and Radhakrishnan *et al.*[28], a trend can be developed. Figure 18 shows the results obtained by the different authors and in this work. The hardness was also adjusted for TiC content by subtracting its alleged contribution to the increase in hardness (which turned out to be minimal). Use was made of the relationship with which Pampuch and Lis determined the hardness of Ti_3SiC_2 from hardness measurements with different TiC contents[14]. As can be seen, more data needs to be collected to really ascertain the relationship between SiC content and hardness. Using the asymptotic values of hardness at higher loads would also be more meaningful.

It is important to note that the increase in Vickers hardness in the composites demonstrates the effect of the reinforcing particles on the pseudoplastic behavior of Ti_3SiC_2. At a load of 98 N, the hardness of Ti_3SiC_2 has reached its asymptotic value of 4 GPa[33]. In contrast, the hardness of the composites is 3 to 4 times that of the monolithic material. Thus, the ability to contain the damage is increased by the presence of the hard particles. They probably hamper the movements of matrix grains aimed at accommodating the stress state created by the indenter. However, once the asymptotic hardness is reached, at 294 N, the hardness is only ~100% (T1600) and ~73% (S1500) more than Ti_3SiC_2. At that load, the presence of the particles does not hinder the movement of Ti_3SiC_2 grains to contain damage as much. However, the effect is still enough that cracks could be developed from the indentation corners on some samples.

Fracture Toughness

The fracture toughness measured on S1500 was found to depend on the formula used to calculate it. The value of a, the half-diagonal of the indentation, was found to be 132.5 μm and the value of c, the distance from the center of the indentation to the extremity of the crack, was found to be 181.7 μm. Young's modulus for Ti_3SiC_2 was used as an approximation. The expression from Evans and Charles[39] yielded a value of 7.3 MPa-$m^{1/2}$ whereas that of Anstis *et al.*[40] yielded 12.8 MPa-$m^{1/2}$.

However, Anstis *et al.* warned that the relationship they developed was valid only for those ceramics that were well-behaved in their indentation response. Soft ceramics such as Ti_3SiC_2 may not be as well-behaved as common ceramics. Furthermore, the requirement that the crack pattern be well developed (c = 2a) was not met in this case, which invalidates the use of this equation. Consequently, the fracture toughness of S1500, the Ti_3SiC_2/SiC composite, was found to be ~ 7.3 MPa-$m^{1/2}$. This value comes from only one measurement, thus it must be taken with caution. However, it gives an idea of what the fracture toughness may be. As for T1600, the average of three measurements was found to be 5.4 ± 0.4 MPa-$m^{1/2}$.

These values are lower than derived for the fine-grained monolithic material from rising resistance-curve behavior. In S1500, transgranular fracture through the SiC particles was found, such as shown in Figure 19. The fracture mode could not be determined in T1600 because TiC cannot be distinguished from Ti_3SiC_2 under the SEM. For the sake of the

argument, it will be assumed that the fracture mode would be the same for TiC particles as for SiC particles in S1500.

The fracture toughness of the reinforcing phases is lower than for Ti_3SiC_2. Since the fracture is transgranular in the reinforcing particles, it could be argued that at least part of the decrease in toughness is due to the lower toughness of the particles. The crack can propagate through the particles much more easily than through the matrix, where many energy absorbing mechanisms are active, such as grain bridging, sliding and bending, as well as delamination of individual grains[35]. Also, the hoop stresses around the particles make the crack propagation that much easier. This should account for much of the loss in fracture toughness.

Comparing the fracture toughness of S1500 with the results obtained by Radhakrishnan is meaningless, because he used Anstis' relationship, and the same restrictions as described earlier most probably apply to the results. Therefore, once again, because of the difference in the methods used to measure the different fracture toughnesses, there is little hope here to find a correlation between volume fraction of SiC or TiC and fracture toughness of the corresponding composites from the current data.

Specific Modulus

The stiffness of the composites was estimated using a rule of mixture. The stiffness of SiC and TiC are, respectively, 415 GPa [43] and 460 GPa[41]. This would yield an estimated elastic modulus of 349 GPa for Ti_3SiC_2/SiC and 362 GPa for Ti_3SiC_2/TiC. Table 5 shows estimates of the specific modulus from the theoretical modulus and measured densities

of the composites. Thus, the specific modulus of the Ti_3SiC_2/SiC composite may increase by about 23% compared to Ti_3SiC_2, whereas the Ti_3SiC_2/TiC composite may increase by 12%. These numbers remain to be confirmed by actual modulus measurements.

D. Conclusions

The flexural strength of the Ti_3SiC_2/SiC and Ti_3SiC_2/TiC composites was found to decrease compared to the monolithic material with similar grain size. This loss of strength was attributed to the thermal expansion mismatch between the reinforcing particles and the matrix. The composites were also found to be damage tolerant with indentation loads up to 98 N, where the transition from microstructure controlled fracture to indentation load controlled fracture occurred. Only the coarser Ti_3SiC_2/SiC composite showed some evidence of thermal shock resistance. All samples seemed to retain similar strength levels after thermal shock. The asymptotic hardness of the Ti_3SiC_2/SiC composite was found to be 6.9 ± 0.7 GPa, while that of the Ti_3SiC_2/TiC composite was 8.2 ± 0.9 GPa. The fracture toughness of Ti_3SiC_2/SiC determined by measurement from a Vickers indentation was found to be ~ 7.3 MPa-m$^{1/2}$. The fracture toughness of Ti_3SiC_2/TiC was found to be 5.4 ± 0.4 MPa-m$^{1/2}$. The lower fracture toughness of the reinforcing particles is thought to be in part responsible for this decrease compared to the monolithic material. The fracture toughness of Ti_3SiC_2/SiC could not be compared to the value obtained by Radhakrishnan due to restrictions on the use of the relationship developed by Anstis *et al.*

III OXIDATION

A. <u>Background</u>

The generic law for growth of an oxide scale can be represented by[44]:

$$\Delta x = K * t^{\,n} \tag{5}$$

where Δx is the oxide scale thickness, K is the growth rate constant and t is the oxidation time. n is a constant whose value usually ranges between 0.5 and 1.0. Δx can be replaced with Δw, the mass change per unit area.

The simplest cases of oxidation are when n is 0.5 or 1.0. In those cases, the oxidation is said to follow a parabolic or linear rate, with the following relationships:

$$\Delta x^{\,2} = K_p * t \tag{6}$$

$$\Delta x = K_{lin} * t \tag{7}$$

K_p is called the parabolic rate constant and K_{lin} the linear rate constant. These rates are representative of the rate-limiting step in the oxidation process. In the case of a parabolic rate, the oxidation is diffusion-controlled. In the case of a linear rate, a chemical reaction in the process is the limiting step. There are also rare cases when n is smaller than 0.5. The oxidation rate is then called logarithmic or subparabolic, and follows the relationship

$$\Delta x = K_{\log} * \ln(1 + t) \tag{8}$$

where $K_{\log}$ is the logarithmic rate constant. This rate law, unlike the preceding ones, does not point to a definite mechanism as the rate-limiting step.

However, in the case of silica forming materials, it has been observed that crystallization within the amorphous silica layer caused a retardation of the oxidation kinetics. Indeed, the diffusion rate of oxygen through cristobalite (one of the crystal structures of silica) is much slower than in amorphous silica. Thus, cristobalite crystals act as barriers to the diffusion of oxygen, reducing the surface area through which oxidation occurs and slowing it down. When the whole surface is covered by a cristobalite layer, the oxidation becomes parabolic again, but at a slower rate.

These three oxidation rate laws are not the answer to all oxidation behaviors. It is often not possible to fit a single law to a set of data because there more than one process is operative during oxidation. That is why many authors have devised other means to fit oxidation data[44-46].

In particular, Nickel[46] devised a multiple-law model whereby the oxide scale thickness is the sum of the contributions of each single law model. Each contribution is determined through the use of multiple linear regressions. The model assumes that all contributions that exist are operative at all times, and does not allow for changes in the kinetics of scale growth.

The oxidation behavior of Ti_3SiC_2 was investigated by many authors[16, 17, 22, 25, 47, 48]. The reports on its oxidation rates varied, but there is a consensus as to the structure of the

oxide scale. It is made of two distinct subscales, an outer porous layer made of TiO_2 (rutile) and an inner layer made of a mix of TiO_2 and SiO_2. Okano and co-workers[17] first reported that the TiO_2 layer was porous and could not be protective. Racault et al.[16] found that the oxidation resistance of Ti_3SiC_2 was better than for TiC under flowing oxygen, noting a positive effect from the presence of silicon atoms compared to TiC, but did not comment on the linearity or parabolic behavior of the oxidation.

Barsoum and El-Raghy[47] were the first to report a parabolic behavior for the oxidation of Ti_3SiC_2 up to 96 hours at 900 and 1000°C, and up to 12 hours from 1240 to 1400°C, with an activation energy of 320 kJ/mol for a sample containing less than 1 mol% TiC, and 370 kJ/mol for a sample that had slightly more impurities. They also reported that the presence of even a little bit of TiC was detrimental to the oxidation resistance of Ti_3SiC_2. Feng et al.[22] investigated the oxidation of Ti_3SiC_2 containing about 2 mol% TiC between 800 and 1100°C for times up to 100 minutes. They found that the oxidation regime from 800 to 950°C was parabolic, with activation energy of 137.7 kJ/mol, whereas from 950 to 1100°C, the activation energy jumped to a value of 312.5 kJ/mol, close to that found by Barsoum and El-Raghy. Radhakrishnan et al.[25] oxidized a sample at 1000°C for 50 hours and found its behavior to be paralinear, starting with a parabolic rate and transitioning to a linear behavior after about 10 hours. Finally, Sun et al.[48] investigated the oxidation of Ti_3SiC_2 containing 7 wt% TiC between 900 and 1300°C up to 20 hours. They found its behavior to be parabolic with an activation energy of 350 kJ/mol. They also found a discontinuous SiO_2 barrier sandwiched in the TiO_2 outer layer, as well as bubbles enriched in Si at its surface. In terms of the Ti_3SiC_2/SiC composites, only Tong et al. reported on the oxidation of their composite that its weight

gain was lower than for monolithic Ti_3SiC_2 at 1000°C up to 10 hours. However, they attributed this lower weight gain to the presence of less volume fraction of Ti_3SiC_2 in the composite than in the monolithic material, rather than a beneficial effect from the presence of SiC.

B. <u>Experimental Details</u>

Each sample was cut into rectangular pieces of various dimensions, but never less than 2 mm in thickness. Samples were placed in a furnace in air, heated to the target temperature at a rate of ~16.6°C/min and held there for the desired amount of time. They were cooled either in the furnace or in ambient air. All samples were first held at ~1000°C for times up to 400 or 800 hours. After comparison between oxide scales thickness, S1500 and T1500 were investigated for further times and other temperatures.

S1500 was oxidized at 925°C up to 100 hours, 1010°C up to 800 hours, and at 1125°C and 1220°C up to 100 hours. T1500 was oxidized at 875°C up to 100 hours, 975°C up to 800 hours, and at 1125°C and 1220°C up to 100 hours.

The oxidized samples were mounted, ground with silicon carbide grinding paper to expose a cross-section of healthy material surrounded by the oxide scale, and polished with diamond suspensions up to 1 μm. Measurement of oxide scale thickness was done in a SEM, on at least 3 sides of each sample, with 10 measurements per side, taken at random points. Both the total scale and the inner layer were measured when clearly distinguishable.

Data was fitted using the multiple-law model developed by Nickel[46], described in the next section.

C. Results and Discussion

Figure 20 shows oxidation data for all samples around 1000°C. Exact temperatures are indicated on the figure. It was found that S1500 and T1500 had better oxidation resistance than their counterparts. S1500 and S1600 showed practically the same resistance, but S1500 was exposed to a slightly higher temperature than S1600. T1500 ended with almost the same oxide scale thickness as T1600 after spending twice the time at temperature. Consequently, S1500 and T1500 were chosen for further oxidation studies. Figures 21 and 22 show backscattered SEM micrographs of the oxide scale on S1500 and T1500 after 97 hours, respectively. S1600 and T1600 showed similar features.

The light outermost phase has been many times identified by X-ray diffraction to be TiO_2 (rutile) [16, 17, 22, 25, 47, 48]. The brightest phase is the innermost Ti_3SiC_2, due to the presence of Ti and Si. The dark phase is either SiC or SiO_2, having lower atomic number than TiO_2. SiO_2 is slightly brighter than SiC because of the presence of oxygen, and can also be distinguished because it forms much finer regions than SiC. Black spots are pores, as they remain black even when contrast and brightness are changed. The only phase not directly distinguishable is TiC, which can be detected by using energy dispersive x-ray analysis (EDX) and performing a Si-map of the region to be investigated.

Data Fitting

Figure 23 shows oxidation data for S1500 from 925°C to 1220°C. Although it may not be evident to the naked eye, the oxidation rates are not parabolic. Trying to fit parabolic curves to the data at all temperatures but 925°C showed a deviation towards linearity after some time, as shown on the graph. At 925°C, the data actually indicated a subparabolic rate.

This non-parabolic behavior could be expected since the oxide scale forms two distinct layers. Each layer could be growing at a different rate. At this point, using Nickel's multiple-law model would be appropriate to determine the contributions of each rate law to the oxide thickness.

The first step was to determine whether any particular rate law was contributing to the overall oxide growth rate. It was assumed that the main contribution was parabolic, as was found by Barsoum *et al.* Use was made of a so-called apparent rate constant, $K_{p,a}$. Starting from the assumption that the only contribution to the scale growth was parabolic, it was calculated by applying the parabolic rate law to each data point:

$$K_{p,a} = \frac{\Delta x}{\sqrt{t}} \tag{9}$$

Plotting $K_{p,a}$ against time on a log-log scale and looking at the trends of the plot reveals whether or not contributions from the other rate laws are made. If the rate law was purely parabolic, the slope of the data would be zero, as $K_{p,a}$ would remain constant. If

there was a linear contribution, the value of $K_{p,a}$ would keep on increasing with time, resulting in a positive slope in the plot. If there was a logarithmic contribution, the value of $K_{p,a}$ would increase a little bit then decrease. It is important to mention here that the numbers do not matter, only the trends are looked at.

Figure 24 shows the log-log plot of $K_{p,a}$ against time for S1500. The data at 925°C shows a decreasing trend. At 1010°C, there is an immediate increase in $K_{p,a}$, followed by a more abrupt increase after ~300 hours. At 1125°C, the same thing happens, but the abrupt increase occurs earlier, after 64 hours. At 1220°C, there is a slight increase in $K_{p,a}$.

From these observations, it can be inferred that there is a logarithmic contribution to the oxidation at 925°C. At 1010°C, there are two linear contributions, one operative from the beginning and the other starting after ~300 hours. At 1125°C, the oxidation starts parabolic, but a linear contribution starts after ~25 hours. At 1220°C, there is a linear contribution active from the beginning.

The data at 925°C up to 100 hours was fitted with the following equation:

$$\Delta x_{925} = 0.50\sqrt{t} + 3.51\ln(1+t) \qquad\qquad R^2 = 0.954 \qquad (10)$$

Figure 25 shows the data collected with the fitted law. The oxide scale thickness after 500 hours was measured in order to confirm the validity of this fit by extrapolating the thickness of the oxide scale. The extrapolation gave an underestimate of the actual scale thickness, but within experimental scatter.

Looking at the data up to 100 hours for the two subscales also plotted in Figure 25, there are two striking features. The first is that the inner subscale data could be fit almost

exactly with a logarithmic law and the outer subscale with a parabolic law. Fitting the

data for the inner subscale with a power law resulted in an exponent of ~0.28. The laws

were found to be:

$$\Delta x_{925,inner} = 3.41 \ln(1 + t) \qquad\qquad R^2 = 0.996 \text{ (11)}$$

$$\Delta x_{925,outer} = 0.53 \sqrt{t} \qquad\qquad R^2 = 0.910 \text{ (12)}$$

These are in agreement with Equation (10).

The second feature is that although the total scale fit was close to the actual value at 500

hours, the thickness of the inner subscale was underestimated and that of the outer scale

was overestimated. Changing the fit of the data to include the data at 500 hours yielded

a change in the fitting parameters as follows:

$$\Delta x_{925,500h} = 0.76 \sqrt{t} + 2.90 \ln(1 + t) \qquad\qquad R^2 = 0.994 \text{ (13)}$$

$$\Delta x_{925,inner,500h} = 0.47 \sqrt{t} + 2.57 \ln(1 + t) \qquad\qquad R^2 = 0.991 \text{ (14)}$$

$$\Delta x_{925,outer,500h} = 0.24 \sqrt{t} + 0.55 \ln(1 + t) \qquad\qquad R^2 = 0.955 \text{ (15)}$$

Figure 26 shows this new fit. Compared to Equation (10), Equation (13) indicates that

with the data at 500 hours came an increase in the parabolic contribution and a decrease

in the logarithmic contribution to the oxide thickness. This is a hint that the subparabolic

law observed may be changing into a parabolic law at longer times. Also, the fit of the

subscales is no longer as clear cut as it was until 100 hours. The appearance of the

logarithmic contribution in the equation for the outer subscale is especially puzzling,

unless it is assumed that it existed before, but was so close in behavior to the parabolic contribution that it was unnoticeable. It is difficult at this point to draw definite conclusions as to the nature of this discrepancy in the data. Further experiments are in progress to try to answer this question.

Figures 27 to 29 show the data for oxidation of S1500 at 1010°C, 1125°C and 1220°C, respectively. As stated before, Nickel's model assumes that all contributing processes are active at all times. Since at 1010°C and 1125°C, a linear process appeared to come into play at a later time, an expression developed by Ogbuji[44] to allow for the phasing in of a process after oxidation has started was used.

It is based on Nickel's model, with the addition of a factor $(t/t)^{\beta}$ in front of the contribution that starts later. τ is a time constant that represents the time at which the contribution becomes fully active. It is taken as the longest time recorded because the factor $(t/t)^{\beta}$ should never be larger than 1, at the risk of multiplying the contribution of the rate law, which would not be realistic. β is a constant that controls how fast the contribution kicks in. Note that the flaw in this model is that the contribution that is started later in this fashion is never completely active until the longest time is achieved. However, the approximation is good enough, considering the high R^2 values achieved by the model.

The data was fit to the following equations:

$$\Delta x_{1010} = 4.35 \sqrt{t} + 0.15\,t + (t/800)\,0.11\,t \qquad R^2 = 0.995 \qquad (16)$$

$$\Delta x_{1125} = 17.3 \sqrt{t} + (t/100)^2\,1.66\,t \qquad R^2 = 0.993 \qquad (17)$$

$$\Delta x_{1220} = 48.6 \sqrt{t} + 1.24\,t \qquad\qquad R^2 = 0.987 \qquad (18)$$

The same process was applied to the oxidation data of T1500. Figure 30 shows the log-log plot of $K_{p,a}$ vs. time. The data at 925°C shows a horizontal trend, while at 975°C and 1125°C, there is a steady increase from the beginning. This translates into a simple parabolic law at 925°C and a linear contribution starting from the beginning at 975°C and 1125 °C. The data at 1220°C was not used because the sides of the samples started bulging after 25 hours, as shown in Figure 31, and no useful data could be gathered.

Figures 32 through 34 show the data at each temperature, with the fitted law. The parabolic and linear components are also plotted when appropriate. The fitted laws were found to be:

$$\Delta x_{875} = 3.94 \sqrt{t} \qquad\qquad R^2 = 0.957 \qquad (19)$$

$$\Delta x_{975} = 12.19 \sqrt{t} + 0.24\,t \qquad\qquad R^2 = 0.992 \qquad (20)$$

$$\Delta x_{1125} = 61.87 \sqrt{t} + 1.00\,t \qquad\qquad R^2 = 0.954 \qquad (21)$$

Table 6 presents the parabolic constants calculated from the parabolic component of each fitted law. Figure 35 plots this data on an Arrhenian plot and the activation energies are shown for each sample. Data for pure Ti_3SiC_2 is shown for reference[47]. The activation energy for S1500 was found to be practically the same as for the oxidation of pure Ti_3SiC_2 (M2), while for T1500 it was somewhat lower. The dependence of K_p on temperature is:

$$K_{p,S1500} = 1.42 \times 10^{16} \ \mu m^2/hr \ \exp\left(\frac{-366 \ kJ/mol - K}{RT}\right) \tag{22}$$

$$K_{p,T1500} = 1.85 \times 10^{14} \ \mu m^2/hr \ \exp\left(\frac{-295 \ kJ/mol - K}{RT}\right) \tag{23}$$

These relationships depend heavily on statistical data. The standard deviation in the activation energies was not computed because it would involve tedious and cumbersome calculations. Because of this, it could be argued that the activation energies for oxidation of both composites are actually the same, within experimental error.

Figure 35 shows that the parabolic constant of S1500 is better than pure Ti_3SiC_2 (M2), but only slightly better than Ti_3SiC_2 that was synthesized with less pure starting powders (M1) at 1000°C. T1500 shows a higher constant, as could be expected from the presence of TiO_2.

It should be emphasized that only the constants were compared, because the existence of the linear contributions in S1500 and T1500 is enough to rule out good oxidation resistance. The exceptions are S1500 at 925°C and T1500 at 875°C, which show subparabolic and parabolic behavior, respectively. However, since this linear contribution exists in both composites, one being better and the other being worse, it can be reasonably assumed that oxidation of Ti_3SiC_2 also contains that linear contribution, such as Radhakrishnan *et al.* found. According to this assumption, the only reason why Barsoum *et al.* may not have found this behavior would be because they did not investigate the oxidation behavior at long enough times.

Physical Processes

It was already pointed out by Barsoum *et al.*[47] that the oxidation of Ti_3SiC_2 proceeded according to the following reaction:

$$Ti_3SiC_2 + 5\ O_2 = 3\ TiO_2 + SiO_2 + 2\ CO(g) \tag{24}$$
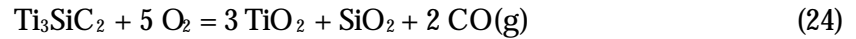
with outward diffusion of titanium and C products and inward diffusion of oxygen. In addition, SiC and TiC particles in the composite oxidize according to the following reactions at the particle/oxide boundary:

$$SiC + O_2 = SiO_2 + C \tag{25}$$

$$TiC + O_2 = TiO_2 + C \tag{26}$$

Deposition of C is believed to be followed by oxidation to CO and outward diffusion.

Following a treatment by Barsoum[49] and assuming that the diffusion of O^{2-} is the limiting step of the parabolic component, the diffusivity of oxygen ions in the composites can be calculated.

The oxidation reaction in Ti_3SiC_2/TiC can be represented by

$$2\ Ti_3SiC_2 + 3\ TiC + 11\ O_2 = 9\ TiO_2 + 2\ SiO_2 + 7\ C \tag{27}$$
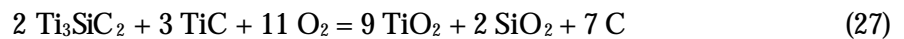
The relative molar quantities of Ti_3SiC_2 and TiC correspond to the volume fraction of TiC.

Since both TiC and Ti₃SiC₂ are oxidized in the Ti₃SiC₂/TiC composite, the first

assumption is that a protective layer of TiO₂ (rutile) is formed. Wagner showed that the

formation of a protective oxide layer in air is given by[50]

$$K_p = -\left(\frac{2kT\Omega_{TiO_2}}{(4e)^2}\right)\frac{\sigma_{ion}\sigma_e}{\sigma_{ion}+\sigma_e}\ln\left(\frac{p_{O_2}}{0.21}\right) \tag{28}$$

where σ_{ion} and σ_e are the average values of the ionic and electronic conductivities across

the layer, and p_{O_2} is the partial pressure of oxygen at the substrate/oxide interface. Ω_{TiO2}

is the atomic volume of TiO₂. k and T have their usual meanings. Using the Nernst-

Einstein relationship, and the fact that when T > 800°C, $\sigma_e \gg \sigma_{ion}$, Equation (28) can be

recast to read

$$D_O = K_p \Big/ \ln\left(\frac{0.21}{p_{O_2}}\right) \tag{29}$$

where D_O is the diffusion coefficient of oxygen and p_{O_2} the partial pressure of oxygen at

the oxide/composite interface. The following assumptions are made in this derivation:

1. SiO₂ acts as an inert phase through which oxygen does not diffuse. This is acceptable

since SiO₂ is much more protective than TiO₂ in terms of oxidation resistance.

2. SiO₂ does not affect the area through which oxygen is diffusing. This assumption is

again valid because of the extra TiO₂ formed from the oxidation of TiC. Thus, the

maximum volume fraction of SiO₂ is reduced to about 22%.

3. The entire growth in the oxide scale is due to the diffusion of O^{2-} ions. This statement is incorrect but the outer subscale never grows thicker than the inner subscale, through which oxygen has to diffuse, so this assumption is off by a factor of 2 at the most.

Assuming local equilibrium, the oxygen partial pressure at the composite/oxide scale interface is fixed by the following reaction

$$2 \ Ti_3SiC_2 + 3 \ TiC + 9 \ O_2 = 9 \ TiO_2 + 2 \ Si + 7 \ C \tag{30}$$
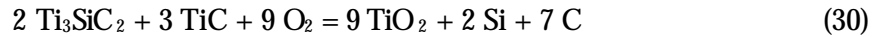
The oxygen partial pressure, p_{O2}, is then given by

$$p_{O2}^9 = a_{Si}^2 \ a_C^7 \ \exp\left(\frac{\Delta G_{rxn}}{R \ T}\right) \tag{31}$$

where ΔG_{rxn} is the standard free energy change of the reaction, and a_x is the activity of the species. ΔG_{rxn} is given by

$$\Delta G_{rxn} = 9\Delta G_{TiO_2} - 2\Delta G_{Ti_3SiC_2} - 3\Delta G_{TiC} \tag{32}$$

The ΔG values are the standard free energies of formation. For Ti_3SiC_2, ΔG is taken from as of yet unpublished work by Barsoum. The rest are taken from the JANAF tables[51].

The activity of Si is assumed to be its molar fraction in the composite. For the activity of C, since TiC does not form at the oxide/substrate interface, the following inequality must hold:

$$a_C \ a_{Ti} \ < \ \exp\left(\frac{\Delta G_{TiC}}{R \ T}\right) \tag{33}$$

The activity of Ti is assumed to be its molar fraction in the composite. This gives an upper bound for the activity of C.

Table 7 shows the quantities used and calculated diffusion coefficients of oxygen ions in the oxide layer at temperatures corresponding to previous data obtained for Ti_3SiC_2[49] (also shown). The calculated diffusion coefficients are of the same order of magnitude as those in the monolithic material. This proves that the parabolic component of oxidation in T1500 is also the diffusion of oxygen in titania.

Oxidation in the Ti_3SiC_2/SiC composite is not as easy to treat as previously done for Ti_3SiC_2/TiC. The main reason is that the SiC particles in the composite oxidize very slowly compared to the matrix. Figure 36 shows S1500 oxidized at 1125°C for 25 hours. It is apparent that the oxidation front in the matrix has advanced past some SiC grains. However, Energy Dispersive X-ray Spectroscopy (EDS) of the SiC grains reveals no trace of oxygen. Consequently, the SiC grains have not yet completely oxidized and act as oxygen diffusion barriers. Because of this, one of the assumptions of the treatment given by Barsoum is no longer valid. Namely, it is the assumption that SiO_2 does not affect the area through which oxygen diffuses. With SiC acting as a diffusion barrier, the starting area of diffusion is reduced by 30% from the start. After SiO_2 has formed, the total volume fraction of diffusion barriers would be ~50%.

The following explanation for the parabolic kinetics of oxidation of S1500 is offered. On Figure 36, the oxidation front has advanced past SiC grains that have not yet oxidized, and Ti_3SiC_2 grains located behind the particles have oxidized. This means that somehow, oxygen ions must have diffused around the SiC grains to reach those regions. If they had

diffused through SiC, they would have oxidized it first. Having to go around randomly dispersed SiC particles would lengthen the diffusion path by a constant factor. The mean diffusion path length thus becomes longer than the thickness of the oxide scale.

Assuming that the diffusion coefficient of oxygen is the same in the composite matrix as in the monolithic material, the resulting parabolic constant would be lower by a constant factor for the composite. One fact in favor of this explanation is the activation energy for parabolic oxidation of the composite and Ti_3SiC_2. It is exactly the same, if experimental scatter is taken into account. Therefore, the ratio of one parabolic constant to the other is a constant. This constant would be related to the factor by which the mean path of diffusion is multiplied due to the presence of SiC particles.

It is acknowledged that this explanation is a departure from Wagner's theory[50], but Wagner's theory was not meant for composite materials, especially when the reinforcing particle does not oxidize. The easiest way to confirm or deny this explanation would be to make a Ti_3SiC_2/SiC composite with parallel SiC fibers instead of particles. If there is to be a confirmation of the above statements, the parabolic rate constants for oxidation of a surface perpendicular to the fibers will be the same as for the monolithic material. If they are lower, then another mechanism will need to be investigated.

The origin of the linear and logarithmic contributions to the oxidation of the composites is not known at present. Some authors have encountered oxidation behavior where the oxidation started according to a parabolic law and transitioned to a linear law[52, 53]. It was explained by the initial formation of a compact oxidation layer, but after some time, some of the oxidation layer would further oxidize into a porous, non-protective oxide,

leading to a linear law. The protective layer would stop growing and the oxidation would become linear.

Figures 37 and 38 show the oxide layer of S1500 oxidized at 1125°C for 9 and 64 hours, respectively. These times are before and after the linear contribution has started taking effect. In both pictures, the oxide layer presents pores throughout the layer. The size and frequency of the pores seem to have increased from 9 hours to 64 hours. Figure 39 shows the oxide scale of T1500 at the same temperature after 64 hours. For this temperature, the linear rate in S1500 was higher than in T1500. Incidentally, the amount of porosity also seems to be higher in S1500. Figures 40 and 41 show the oxide scale of T1500 and S1500 at the lowest temperature tested, where the oxidation was found to be parabolic and subparabolic, respectively. The presence of pores is undeniable, although not in high concentrations. Qualitatively, it seems that the amount of porosity could affect the linear rate contribution, but judging by eye is not reliable. Porosity measurements should be made in order to ascertain any effect on the linear rate of oxidation.

More importantly than pores, however, is the effect of micro-cracks. It has been shown by Barsoum *et al.*[47] that the Pilling-Bedworth ratio of Ti_3SiC_2 is 1.85. In the composites, this ratio should be similar to that number. This volume expansion develops compressive stresses in the oxide layer and tensile stresses in the healthy material, especially since the oxide scale adheres to the samples. Since these stresses are developed rather slowly, the formation of micro-cracks ahead of the oxidation front is possible. These micro-cracks would allow oxygen to diffuse faster into the healthy material, hastening the oxidation rate and possibly resulting in the linear contribution to the oxide scale growth. They were not found upon observation of the oxide scale under

the SEM, but they may be too small to be detected, because they do not really open up before oxidation takes place.

D. <u>Conclusions</u>

The composites Ti_3SiC_2/SiC and Ti_3SiC_2/TiC were oxidized at temperatures ranging from 875°C to 1220°C. The oxidation behaviors were fitted using Nickel's multiple law model. The Ti_3SiC_2/SiC composite showed subparabolic oxidation behavior at 925°C up to 500 hours. Further experimentation will show whether this behavior will remain subparabolic. At higher temperatures, the oxidation behavior was paralinear, starting parabolically, but transitioning to a linear regime. The Ti_3SiC_2/TiC composite showed parabolic oxidation behavior at 875°C and paralinear behavior at higher temperatures. At 1220°C, it oxidized catastrophically. The parabolic component of the oxidation behavior of the composites was shown to depend on diffusion of oxygen through the oxide layer. The parabolic constants of the Ti_3SiC_2/SiC composite were lower than for the monolithic material, and those of the Ti_3SiC_2/TiC composite higher. The linear process may be caused by the formation of micro-cracks ahead of the oxidation front, but they could not be observed under the SEM, possibly because of their small size. The subparabolic oxidation contribution could not be determined.

IV SUMMARY AND RECOMMENDATIONS

Ti_3SiC_2/SiC and Ti_3SiC_2/TiC composites were fabricated by HIPing. Their microstructure was controlled by the presence of the reinforcing particles.

The mechanical properties of the materials were diversely affected by the presence of the reinforcements, compared to the monolithic material. The strength and fracture toughness were found to decrease, whereas the hardness and damage tolerance increased. In particular, the damage tolerance proved to be higher by at least an order of magnitude compared to conventional ceramics. The specific modulus was also thought to increase because of the increase in estimated stiffness and/or decrease in density of the composites. The actual stiffness has yet to be measured.

The oxidation resistance of the Ti_3SiC_2/SiC composite was also better than that of Ti_3SiC_2, with a subparabolic behavior at 925°C. The Ti_3SiC_2/TiC composite, however, showed worse resistance, as was expected.

After reviewing the data obtained on the properties of the composites, it is recommended that the properties of the Ti_3SiC_2/SiC composite be further explored. Its improved oxidation resistance, specific modulus and damage tolerance make it a worthwhile contender for high temperature applications, at least up to 925°C. Factors such as the effect of volume fraction of particles or the use of SiC whiskers instead of particles should be explored in order to optimize the properties of the composite.

LIST OF REFERENCES

1. Jeitschko, W. and Nowotny, H., *Die Kristallstructur von Ti₃SiC₂ - Ein Neuer Komplxcarbid-Typ,* Monatsh. fur Chem., **98**, 2401 (1967)

2. Wolfsgruber, H., Nowotny, H., and Benesovsky, F., *Die Kristallstruktur von Ti₃GeC₂,* Monatsh. fur Chem., **98**, 2401 (1967)

3. Pietzka, M.A. and Schuster, J.C., *Summary of Constitution Data of the System Al-C-Ti,* J. Phase Equilibria, **15**, 392 (1994)

4. Pietzka, M.A. and Schuster, J.C. *The Ternary Boundary Phases of the Quaternary System Ti-Al-C-N.* in *Concerted Action on Materials Science, Leuven Proceedings, Part A.* 1992. Brussels, Belgium.

5. Nickl, J.J., Schweitzer, K.K., and Luxenberg, P., *Gasphasenabscheidung im Systeme Ti-C-Si,* J. Less Common Metals, **26**, 283 (1972)

6. Goto, T. and Hirai, T., *Chemically Vapor Deposited Ti₃SiC₂,* Materials Research Bulletin, **22**, 1195-1201 (1987)

7. Racault, C., Langlais, F., Naslain, R., and Kihn, Y., *On the Chemical Vapour Deposition of Ti₃SiC₂ from TiCl₄-SiCl₄-CH₄-H₂ Gas Mixtures: Part II An Experimental Approach,* J. Mater. Sci., **29**, 3941 (1994)

8. Racault, C., Langlais, F., and Bernard, C., *On the Chemical Vapour Deposition of Ti₃SiC₂ from TiCl₄-SiCl₄-CH₄-H₂ Gas Mixtures: Part I A Thermodynamic Approach,* J. Mater. Sci., **29**, 5023 (1994)

9. Pickering, E., Lackey, W.J., and Crain, S., *Microstructure of Ti₃SiC₂ Coatings Synthesized by CVD,* Ceram. Trans. 96, Advances in Ceramic Matrix Composites IV, Eds. J. P. Singh and N. Bansal,, (1999)

10. Pampuch, R., Lis, J., Stobierski, L., and Tymkiewicz, M., *Solid Combustion Synthesis of Ti₃SiC₂,* J. Europ. Ceram. Soc., **5**, 283 (1989)

11. Lis, J., Pampuch, R., and Stobierski, L., *Reactions During SHS in a Ti-Si-C System,* Int. J. of Self-Propagating High-Temp. Synth., **1**, 401 (1992)

12. Lis, J., Pampuch, R., Piekarczyk, J., and Stobierski, L., *New Ceramics Based on Ti₃SiC₂,* Ceramics International, **19**, 219 (1993)

13.   Pampuch, R., Lis, J., Piekarczyk, J., and Stobierski, L., *Ti$_3$SiC$_2$-Based Materials Produced by Self-Propagating High Temperature Synthesis and Ceramic Processing,* J. Mater. Synth. and Process., **1**, 93 (1993)

14.   Lis, J., Miyamoto, Y., Pampuch, R., and Tanihata, K., *Ti$_3$SiC$_2$-Based Materials Prepared by HIP-SHS Techniques,* Materials Letters, **22**, 163-168 (1995)

15.   Morgiel, J., Lis, J., and Pampuch, R., *Microstructure of Ti$_3$SiC$_2$-based Ceramics,* Materials Letters, **27**, 85 (1996)

16.   Racault, C., Langlais, F., and Naslain, R., *Solid-state Synthesis and Characterization of the Ternary Phase Ti$_3$SiC$_2$,* J. Mater. Sci., **29**, 3384 (1994)

17.   Okano, T., Yano, T., and Iseki, T., *Synthesis and Mechanical Properties of Ti$_3$SiC$_2$ Ceramic,* Trans. Mat. Res. Soc. Japan, **14A**, 597 (1993)

18.   Arunajatesan, S. and Carim, A., *Synthesis of Ti$_3$SiC$_2$,* J. Amer. Cer. Soc., **78**, 667 (1995)

19.   Barsoum, M.W. and El-Raghy, T., *Synthesis and Characterization of a Remarkable Ceramic: Ti$_3$SiC$_2$,* J. Amer. Cer. Soc., **79**, 1953 (1996)

20.   Gao, N.F., Miyamoto, Y., and Tanihata, K., *Synthesis of Highly Dense Ti$_3$SiC$_2$ by HIP and its Characterization,* J. Soc. Mater. Sci. Jap., **47**(10), 994-999 (1998)

21.   Goesmann, F., Wenzel, R., and Schmid-Fetzer, R., *Preparation of Ti$_3$SiC$_2$ by Electron-Beam-Ignited Solid-State Reaction,* J. Amer. Cer. Soc., **81**(11), 3025-3028 (1998)

22.   Feng, A., Orling, T., and Munir, Z.A., *Field-Activated Pressure-Assisted Combustion Synthesis of Polycrystalline Ti$_3$SiC$_2$,* J. Mater. Res., **14**(3), 925-939 (1999)

23.   Li, J.F., Sato, F., and Watanabe, R., *Synthesis of Ti$_3$SiC$_2$ Polycrystals by Hot-Isostatic Pressing of the Elemental Powders,* J. Mater. Sci. Lett., **18**(19), 1595-1597 (1999)

24.   Li, J.T. and Miyamoto, Y., *Fabrication of Monolithic Ti$_3$SiC$_2$ Ceramic through Reactive Sintering of Ti/Si/2TiC,* J. Mater. Synth. and Process., **7**(2), 91-96 (1999)

25.   Radhakrishnan, R., Williams, J.J., and Akinc, M., *Synthesis and High-Temperature Stability of Ti$_3$SiC$_2$,* J. of Alloys and Compounds, **285**, 85-88 (1999)

26.   Tang, K., Wang, C., Huang, Y., and Xia, J., *An X-Ray Diffraction Study of the Texture of Ti$_3$SiC$_2$ Fabricated by Hot Pressing,* J. Europ. Ceram. Soc., **21**, 617-620 (2001)

27.   Tong, X., Okano, T., Iseki, T., and Yano, T., *Synthesis and High Temperature Mechanical Properties of Ti$_3$SiC$_2$/SiC Composite,* J. Mater. Sci., **30**, 3087-3090 (1995)

28. Radhakrishnan, R., Henager, C.H.J., Brimball, J.L., and Bhaduri, S.B., *Synthesis of Ti₃SiC₂/SiC and TiSi₂/SiC Composites Using Displacement Reactions in the Ti-Si-C System,* Scripta Materialia, **34**(12), 1809-1814 (1996)

29. El-Raghy, T. and Barsoum, M.W., *Processing and Mechanical Properties of Ti₃SiC₂: I, Reaction Path and Microstructure Evolution,* J. Amer. Cer. Soc., **82**(10), 2849-2854 (1999)

30. Yang, S.C., Higgins, G.T., and Nash, P., *Coarsening kinetics of solid and liquid silver particles in nickel,* Materials Science and Technology, **8**, 10-15 (1992)

31. Barsoum, M.W., Brodkin, D., and El-Raghy, T., *Layered Machinable Ceramics for High Temperature Applications,* Scripta Materialia, **36**(5), 535-541 (1997)

32. El-Raghy, T., Zavaliangos, A., Barsoum, M.W., and Kalidindi, S.R., *Damage Mechanisms Around Hardness Indentations in Ti₃SiC₂,* J. Amer. Cer. Soc., **80**, 513-516 (1997)

33. El-Raghy, T., Barsoum, M.W., Zavaliangos, A., and Kalidindi, S.R., *Processing and Mechanical Properties of Ti₃SiC₂: II, Effect of Grain Size and Deformation Temperature,* J. Amer. Cer. Soc., **82**(10), 2855-2860 (1999)

34. Barsoum, M.W., El-Raghy, T., and Radovic, M., *Ti3SiC2: A Layered Machinable Ductile Carbide,* Interceram, **49**, 226-233 (2000)

35. Gilbert, C.J., et al., *Fatigue-Crack Growth and Fracture Properties of Coarse and Fine-Grained Ti₃SiC₂,* Scripta Materialia, **42**, 761-767 (2000)

36. Chen, D., et al., *Cyclic Fatigue-Crack Growth and Fracture Properties in Ti₃SiC₂ Ceramics at Elevated Temperatures,* J. Amer. Cer. Soc., **84**(12), 2914-2920 (2001)

37. Li, J.F., Pan, W., Sato, F., and Watanabe, R., *Mechanical Properties of Polycrystalline Ti₃SiC₂ at Ambient and Elevated Temperatures,* Acta Materialia, **49**, 937-945 (2001)

38. *Standard Test Method for Flexural Strength of Advanced Ceramics at Ambient Temperature,* ASTM Designation C1161-94. American Society for Testing and Materials, West Conshohocken, PA.

39. Evans, A.G. and Charles, E.A., *Fracture Toughness Determination by Indentation,* J. Amer. Cer. Soc., **59**(7-8), 371-372 (1976)

40. Anstis, G.R., Chantikul, P., Lawn, B.R., and Marshall, D.B., *A Critical Evaluation of Indentation Techniques for Measuring Fracture Toughness: I, Direct Crack Measurements,* J. Amer. Cer. Soc., **64**(9), 533-538 (1981)

41. Pierson, H.O., *Handbook of Refractory Carbides and Nitrides.* 1996, Westwood, NJ: Noyes Publications.

42.	Cook, R.F., Lawn, B.R., and Fairbanks, C.J., *Microstructure-Strength Properties in Ceramics: I, Effect of Crack Size on Toughness,* J. Amer. Cer. Soc., **68**(11), 604-615 (1985)

43.	Munro, R.G., *Materials Properties of a Sintered alpha-SiC,* J. Phys. and Chem. Ref. Data, **26**, 1195-1203 (1997)

44.	Ogbuji, L., *Subparabolic Oxidation Behavior of Silicon Carbide at 1300°C,* J. Electrochem. Soc., **145**(8), 2876-2882 (1998)

45.	Kall, P.-O., Nygren, M., and Persson, J., *Non-Parabolic Oxidation Kinetics of Advanced Ceramics,* in *Corrosion of Advanced Ceramics: Measurement and Modelling,* K.G. Nickel, Editor. 1994, Kluwer Academic Publishers: Netherlands. p. 73-84.

46.	Nickel, K.G., *Multiple Law Modelling for the Oxidation of Advanced Ceramics and a Model-Independent Figure of Merit,* in *Corrosion of Advanced Ceramics: Measurement and Modelling,* K.G. Nickel, Editor. 1994, Kluwer Academic Publishers: Netherlands. p. 59-71.

47.	Barsoum, M.W., El-Raghy, T., and Ogbuji, L., *Oxidation of Ti_3SiC_2 in Air,* J. Electrochem. Soc., **144**, 2508 (1997)

48.	Sun, Z., Zhou, Y., and Li, M., *Oxidation Behaviour of Ti_3SiC_2-Based Ceramic at 900-1300°C in Air,* Corrosion Science, **43**, 1095-1109 (2001)

49.	Barsoum, M.W., *Oxidation of $Ti_{n+1}AlX_n$ (n = 1-3 and X = C, N), I. Model,* J. Electrochem. Soc., **148**(8), C544-C550 (2001)

50.	Wagner, C., Z. Phys. Chem. Abt. B, **21**, 25 (1933)

51.	Chase, M.W., et al., *JANAF Thermodynamic Tables, 3rd ed.,* J. Phys. and Chem. Ref. Data, **14**(Suppl. 1) (1985)

52.	Webb, W.W., Norton, J.T., and Wagner, C., *Oxidation of Tungsten,* J. Electrochem. Soc., **103**(2), 107-111 (1956)

53.	Smeltzer, W.W. and Simnad, M.T., *Oxidation of Hafnium,* Acta Metallurgica, **5**, 328-334 (1957)

54.	Barsoum, M.W., *The $M_{N+1}AX_N$ Phases: A New Class of Solids; Thermodynamically Stable Nanolaminates,* Prog. Solid St. Chem., **28**, 201-281 (2000)

APPENDIX A   TABLES

Table 1: List of ternary compounds belonging to the $M_{n+1}AX_n$ family[54]

IIB	IIIA	IVA	VA	VIA
	Al	**Si**	**P**	**S**
	Ti_2AlC	Ti_3SiC_2 4.52	V_2PC	Ti_2SC
	V_2AlC	(3.0665,17.671)	Nb_2PC	Zr_2SC
	Cr_2AlC			$Nb_2SC_{0.4}$
	Nb_2AlC			Hf_2SC
	Ta_2AlC			
	Ti_2AlN			
	Ti_3AlC_2			
	Ti_4AlN_3			
Zn	**Ga**	**Ge**	**As**	**Se**
	Ti_2GaC	Ti_2GeC	V_2AsC	
	V_2GaC	Cr_2GeC	Nb_2AsC	
	Cr_2GaC	Cr_2GeC		
	Nb_2GaC	Ti_3GeC_2		
	Mo_2GaC			
	Ta_2GaC			
	Ti_2GaN			
	Cr_2GaN			
	V_2GaN			
Cd	**In**	**Sn**	**Sb**	**Te**
Ti_2CdC	Sc_2InC	Ti_2SnC		
	Ti_2InC	Zr_2SnC		
	Zr_2InC	Nb_2SnC		
	Nb_2InC	Hf_2SnC		
	Hf_2InC	Hf_2SnN		
	Ti_2InN			
	Zr_2InN			
	Tl	**Pb**	**Bi**	
	Ti_2TlC	Ti_2PbC		
	Zr_2TlC	Zr_2PbC		
	Hf_2TlC	Hf_2PbC		
	Zr_2TlN			

Table 2: Theoretical and measured densities of the samples

Sample	SiC Vol%	TiC Vol%	Theor. D. (g/cm^3)	Meas. D. (g/cm^3)	Rel. D. (%)
S1600	30	4	4.15	4.09	98.6
S1500	30	3	4.14	4.02	97.1
T1600	3	30	4.60	4.58	99.6
T1500	1	29	4.62	4.49	97.0

Table 3: Selected results from 4-point bend tests. Results for monolithic Ti$_3$SiC$_2$ from Ref. 33

Sample	Strength (MPa)	Thermal Shock T = 1400°C	Damage Tolerance Load = 294N
Ti$_3$SiC$_2$ (CG)	330	300	230
Ti$_3$SiC$_2$ (FG)	600	---	442
S1600	218 ± 9	190 ± 7	178 ± 6
S1500	315 ± 5	241 ± 22	230 ± 25
T1600	365 ± 14	229 ± 20	280 ± 23
T1500	375 ± 47	---	---

Table 4: Retained strength after thermal shock from indicated temperature

Sample	As Processed	700°C	1000°C	1200°C	1400°C
S1600	218 ± 9	220 ± 23	173 ± 24	194 ± 31	190 ± 7
S1500	315 ± 5	230 ± 17	207 ± 21	199 ± 26	241 ± 22
T1600	365 ± 14	217 ± 19	189 ± 57	226 ± 41	229 ± 20

Table 5: Estimation of specific modulus of the composites

Sample	Elastic Modulus (GPa)	Density (g/cm^3)	Specific Modulus (GPa/(g/cm^3))	Increase from Ti$_3$SiC$_2$
Ti$_3$SiC$_2$	320	4.53	70.6	---
S1500	349	4.02	86.8	23%
T1600	362	4.58	79.0	12%

Table 6: Parabolic rate constants for oxidation of S1500 and T1500

S1500		T1500	
T (^{o}C)	K$_p$ (μm^2/hr)	T (^{o}C)	K$_p$ (μm^2/hr)
1010	18.92	875	7.76
1125	299.29	975	74.30
1220	2361.96	1125	1913.95

Table 7: Estimation of oxygen diffusion coefficients in T1500. Data for Ti$_3$SiC$_2$ from Ref. 49

Sample	Temp. (^{o}C)	K$_p$ (m^2/s)	a$_{Si}$	a$_{Ti}$	a$_C$	ΔG_{rxn} (kJ/mol)	P$_{O2}$ (atm)	**D$_{O^{2-}}$ (m^2/s)**
T1500	875	1.9E-15	0.111	0.5	5.7E-06	-5416.1	2.1E-32	**2.7E-17**
	900	3.7E-15	0.111	0.5	7.3E-06	-5377.8	1.5E-31	**5.3E-17**
	1000	4.0E-14	0.111	0.5	1.8E-05	-5223.9	1.8E-28	**6.4E-16**
Ti$_3$SiC$_2$	900	9.0E-16	0.167	0.5	4.9E-08	---	7.3E-31	**1.3E-17**
	1000	6.9E-15	0.167	0.5	2.5E-07	---	9.5E-28	**1.1E-16**

APPENDIX B   FIGURES
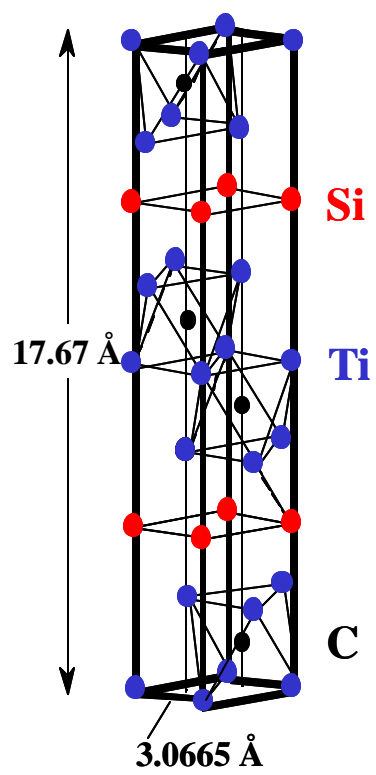
Figure 1: Unit cell of Ti$_3$SiC$_2$
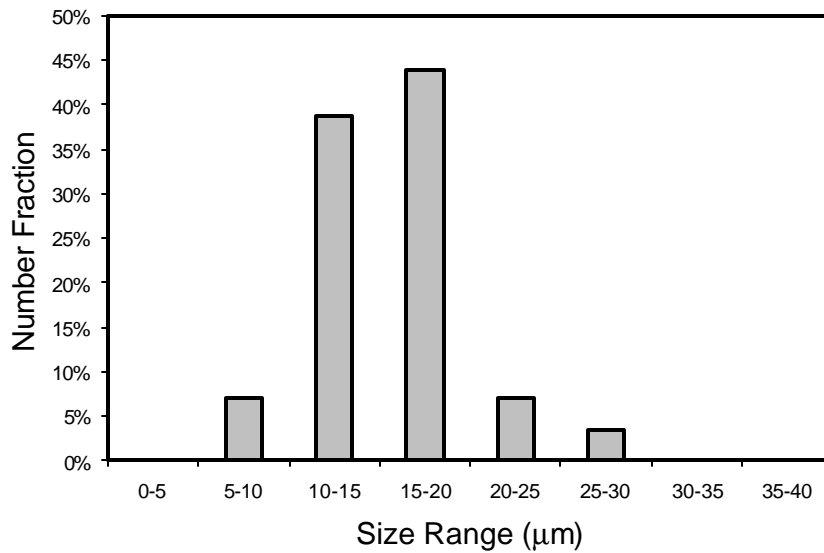
Figure 2: Particle size distribution of SiC powder used in S1600 and T1600
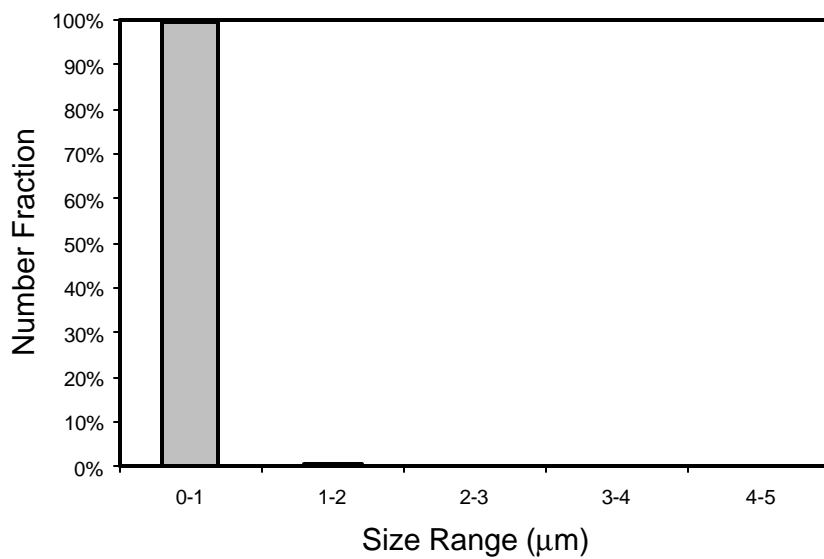
Figure 3: Particle size distribution of SiC powder used in S1500 and T1500
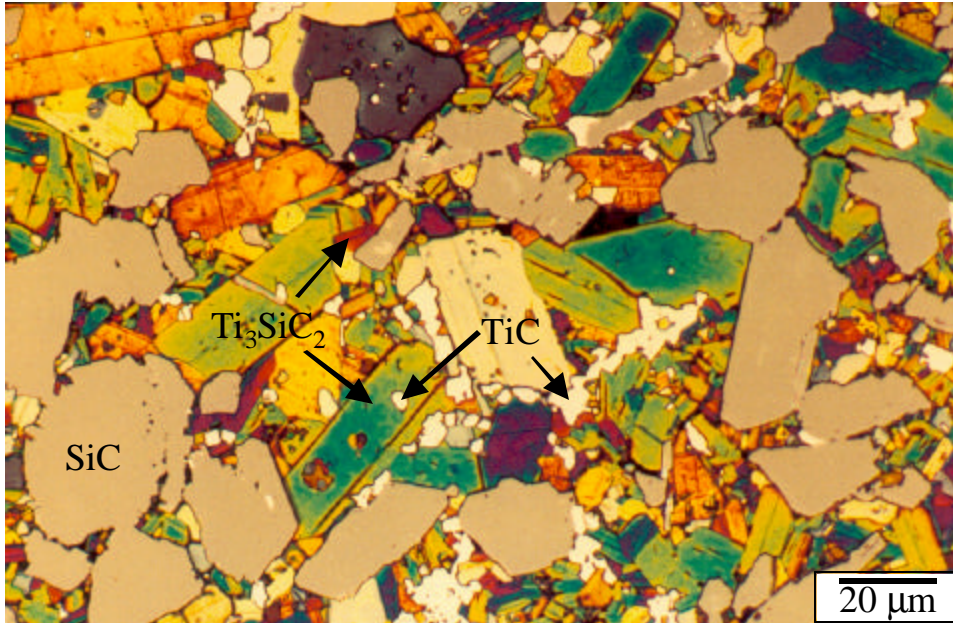
Figure 4: Representative cross-section of sample S1600
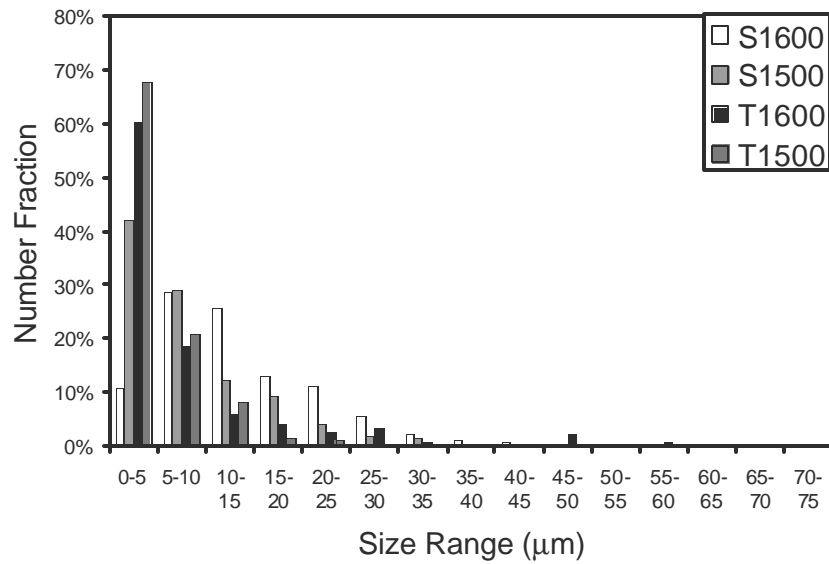
Figure 5: Grain size distribution of reinforcing phases in the composites
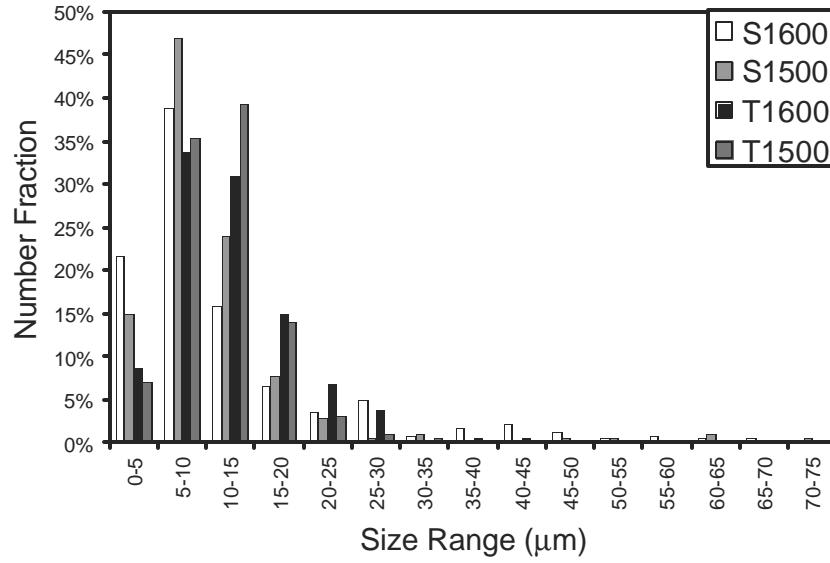
Figure 6: Grain size distribution of Ti$_3$SiC$_2$ matrix in the composites
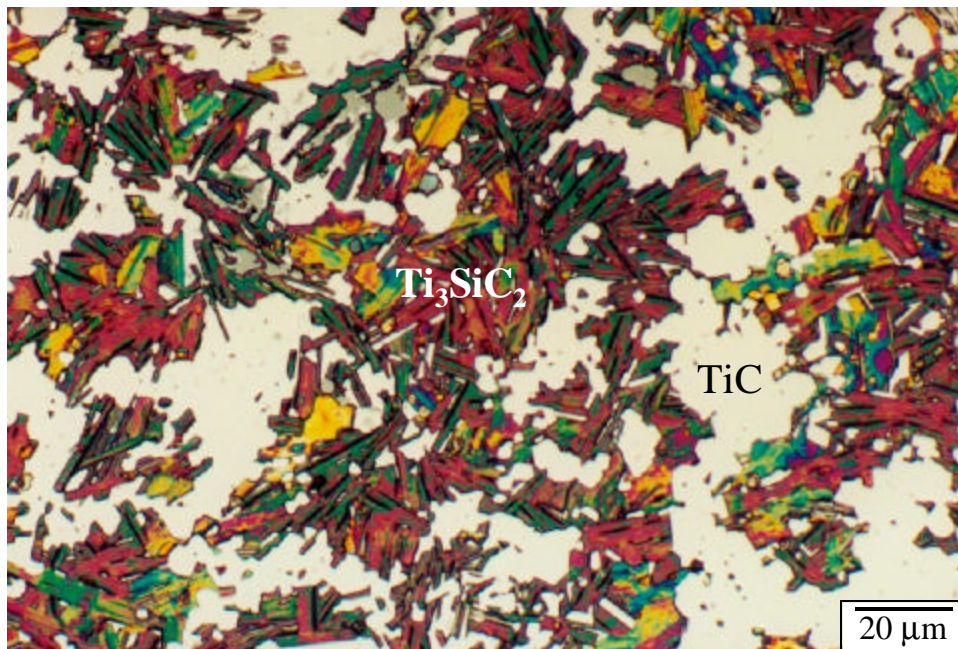
Figure 7: Representative cross-section of sample T1600
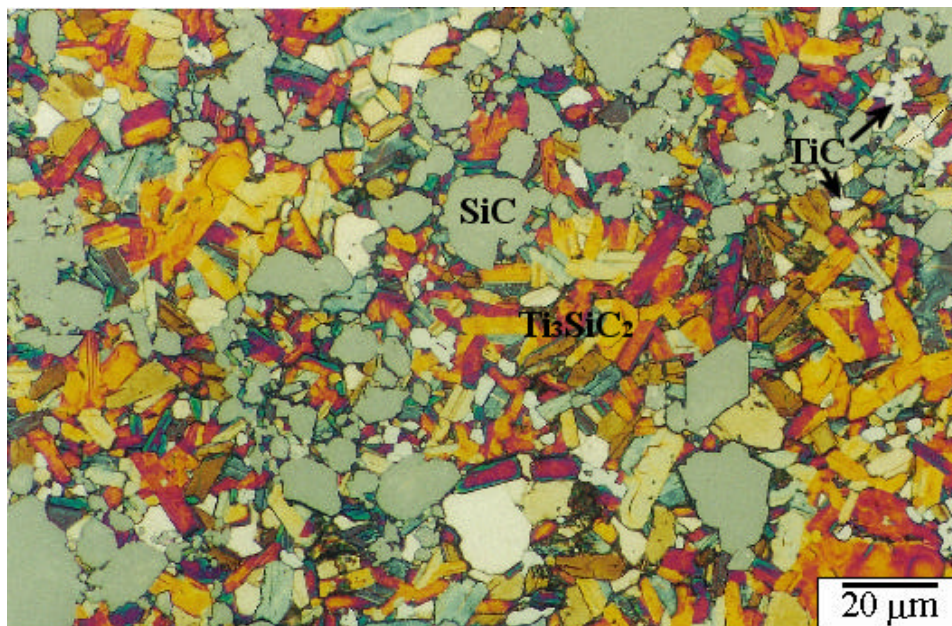
Figure 8: Representative cross-section of sample S1500
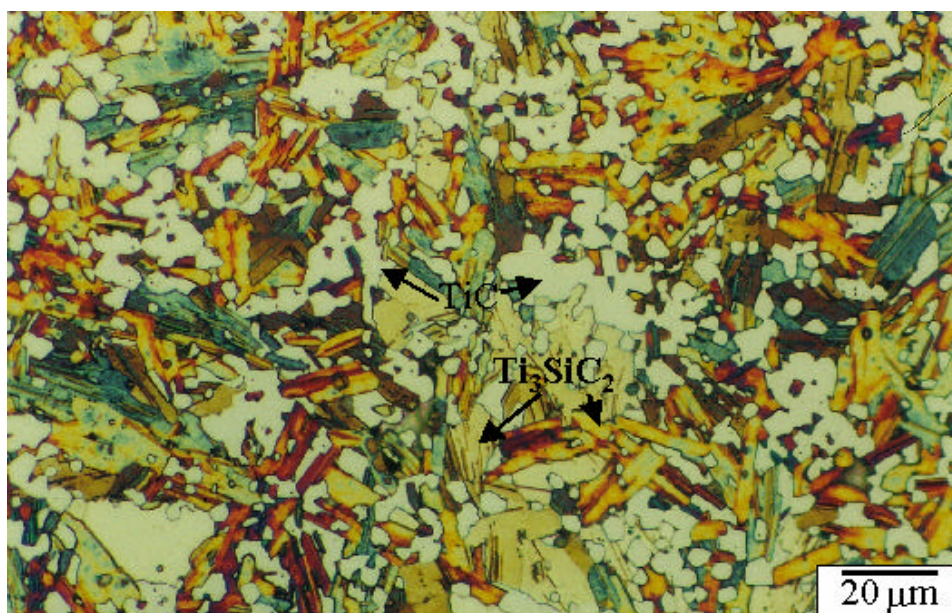
Figure 9: Representative cross-section of sample T1500
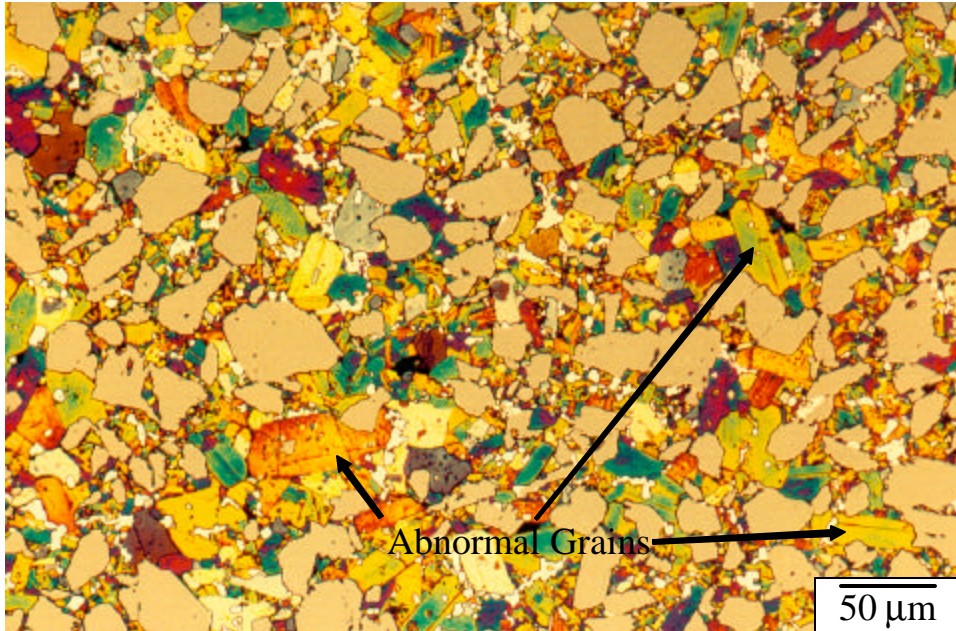
Figure 10: Example of abnormal grain growth in S1600
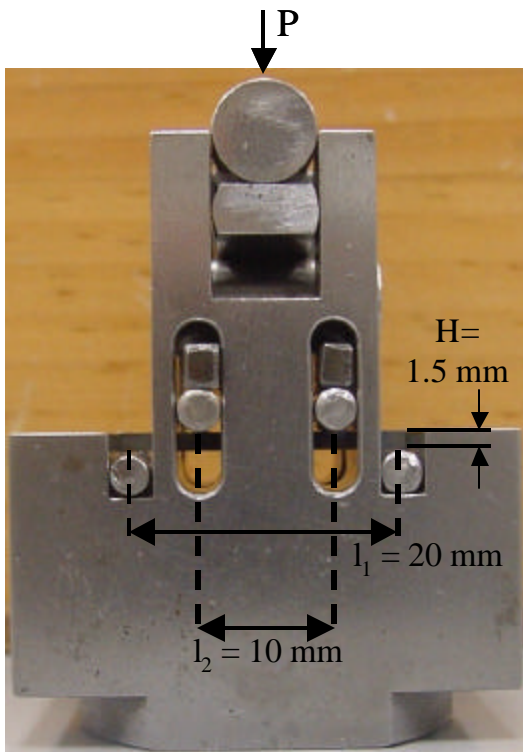
Figure 11: Four-point bend stainless steel fixture with relevant dimensions
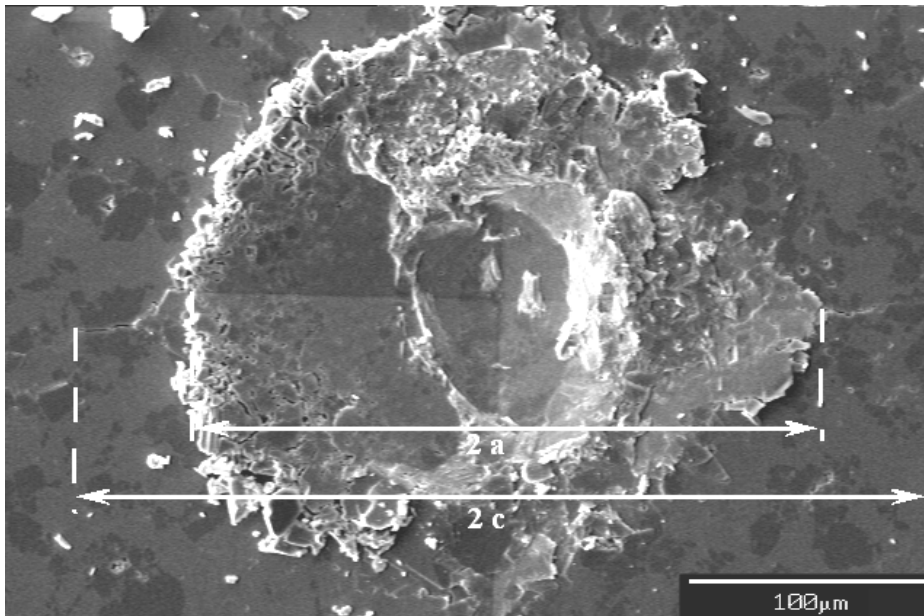
Figure 12: Vickers indentation (P = 30kg) on S1500 showing cracks emanating from the corners
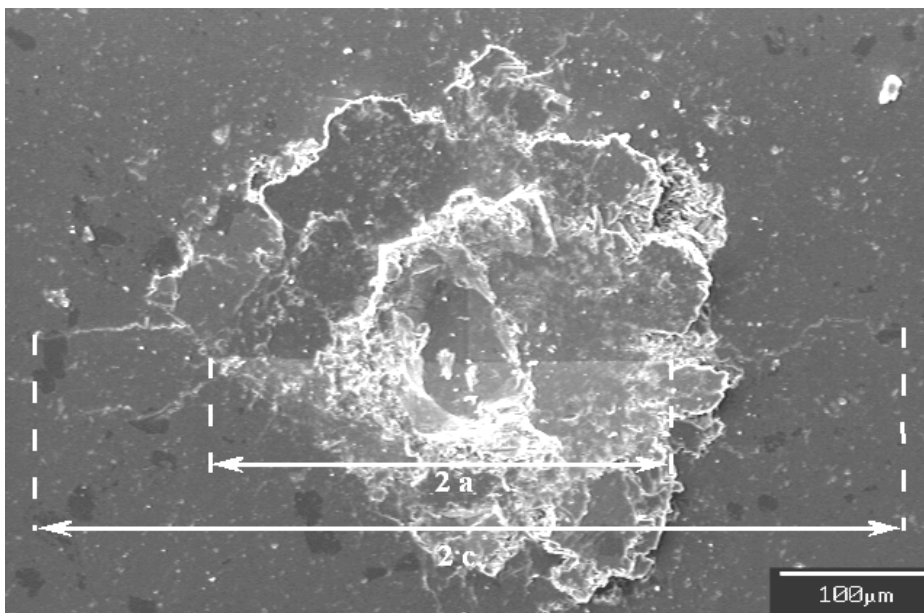
Figure 13: Vickers indentation (P = 50kg) on T1600 showing cracks emanating from the corners
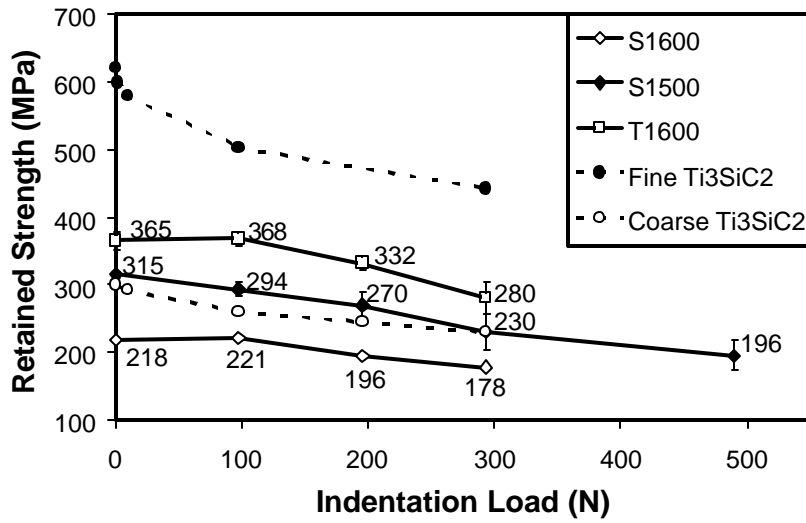
Figure 14: Damage tolerance chart. Data for monolithic Ti$_3$SiC$_2$ from Ref. 33
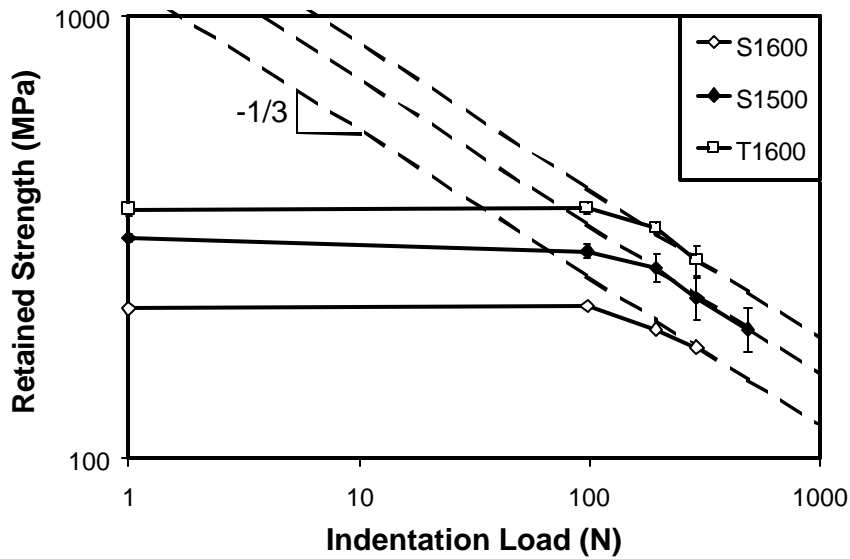
Figure 15: Log-log plot of damage tolerance data. Dotted lines represent dependence of retained strength on the applied load (P$^{-1/3}$)
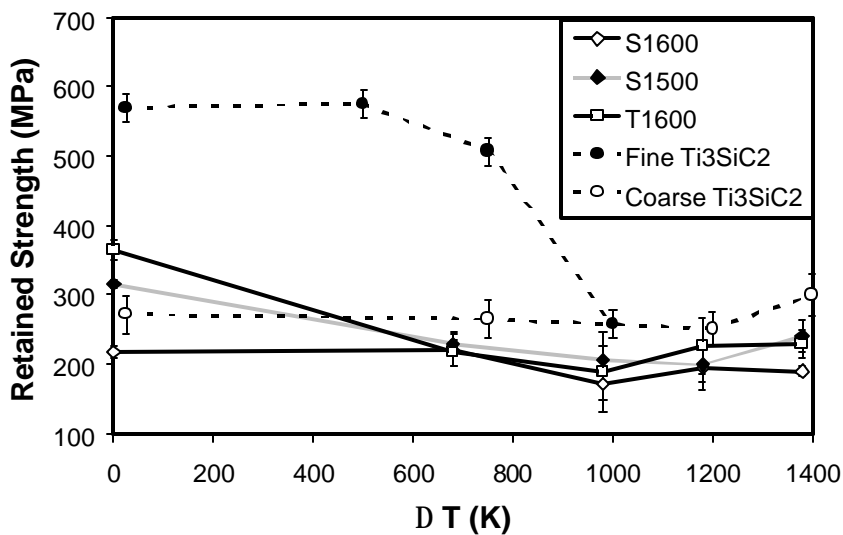
Figure 16: Thermal shock resistance chart. Data for monolithic Ti$_3$SiC$_2$ from Ref. 33

	98 N	196 N	294 N	490 N
S1600	16.3 ± 2.2	6.4 ± 0.8	7.2 ± 1.1	---
S1500	11.3 ± 2.3	6.6 ± 0.7	7.2 ± 0.8	6.9 ± 0.7
T1600	15.2 ± 2.7	14.3 ± 5.6	8.3 ± 1.4	8.2 ± 0.9
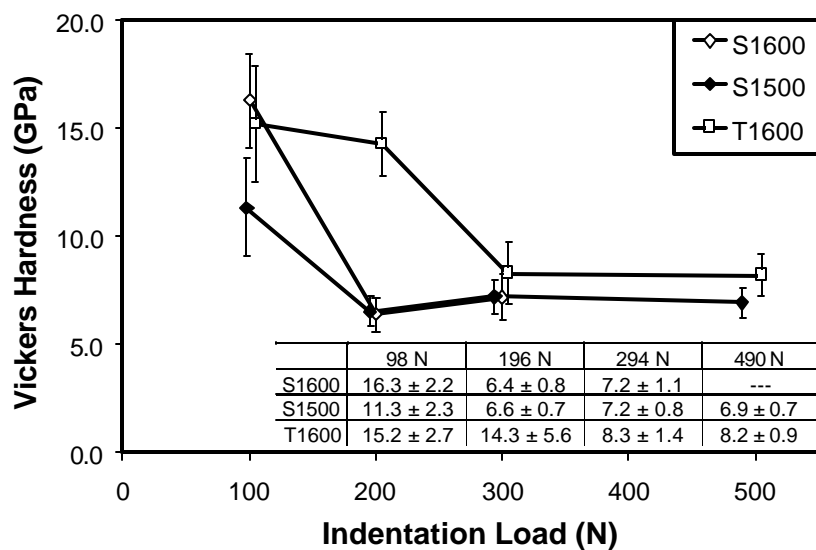
Figure 17: Vickers hardness as a function of indentation load (results shifted for clarity)
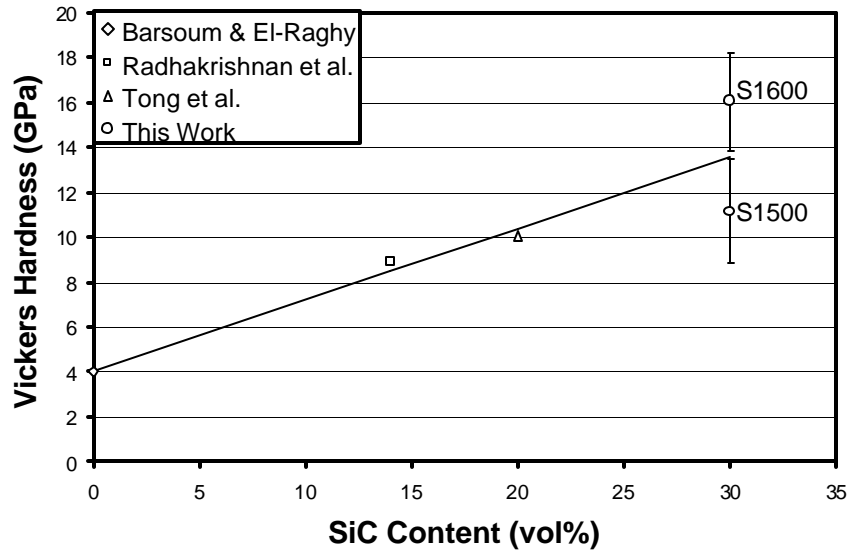
Figure 18: Variation of hardness at 98 N with SiC content
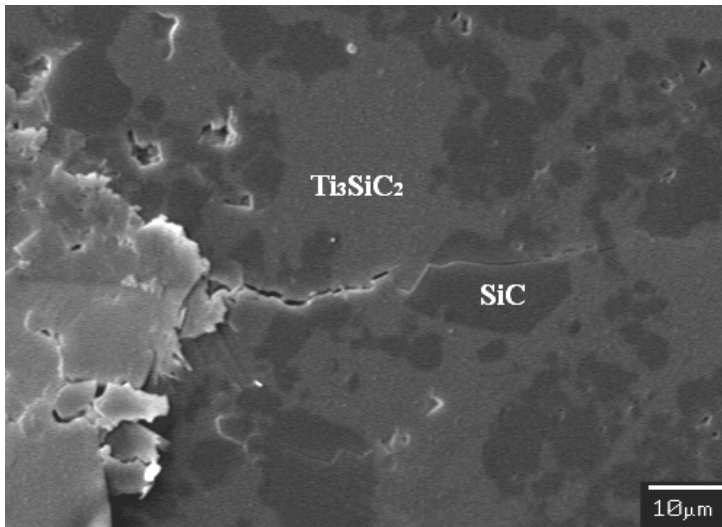
Figure 19: Crack developed from indentation corner on S1500
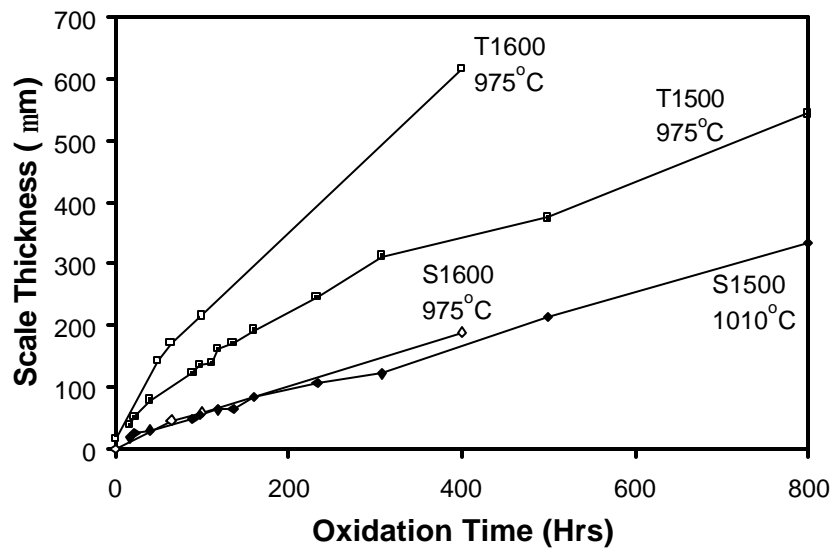
Figure 20: Oxidation of all samples around 1000°C
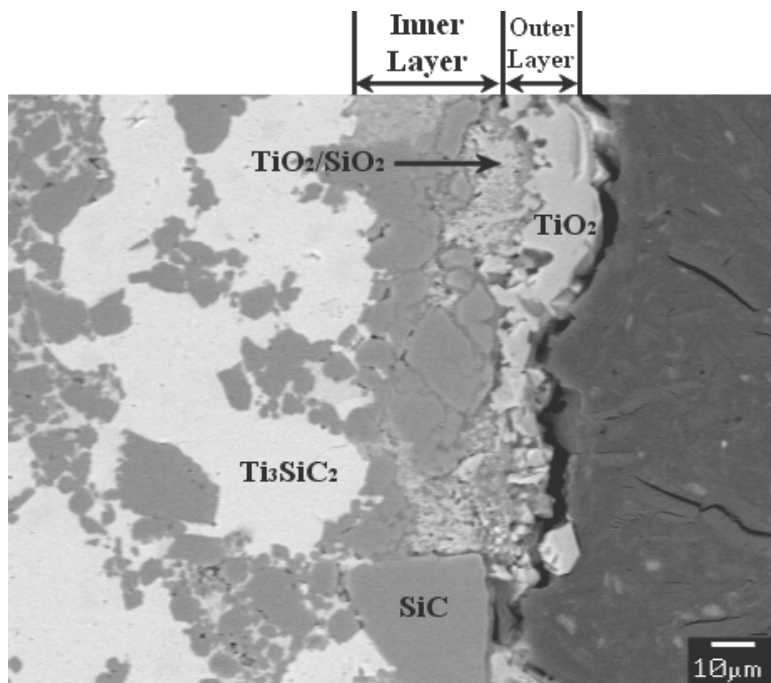
Figure 21: Oxide scale of S1500 after 97 hours at 1010°C
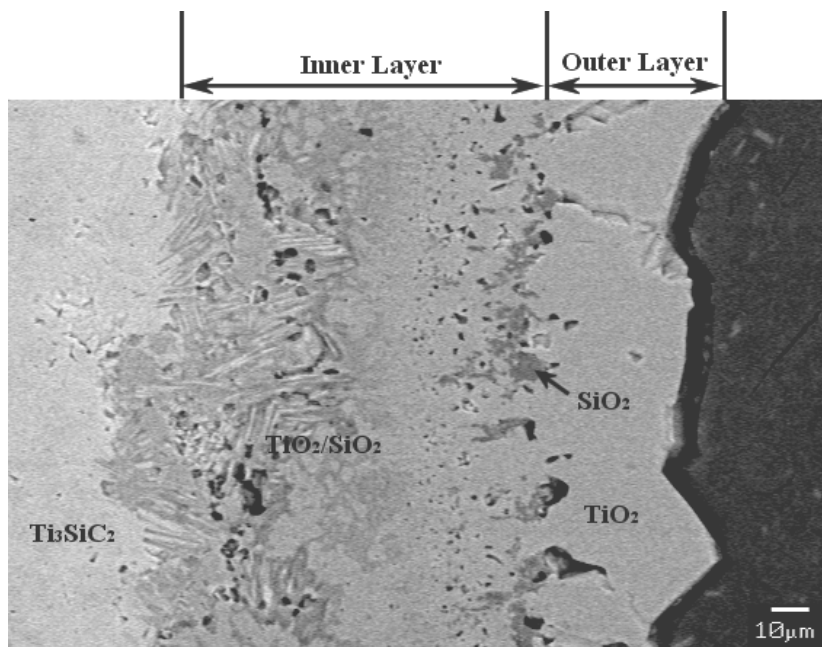
Figure 22: Oxide scale of T1500 after 97 hours at 975°C
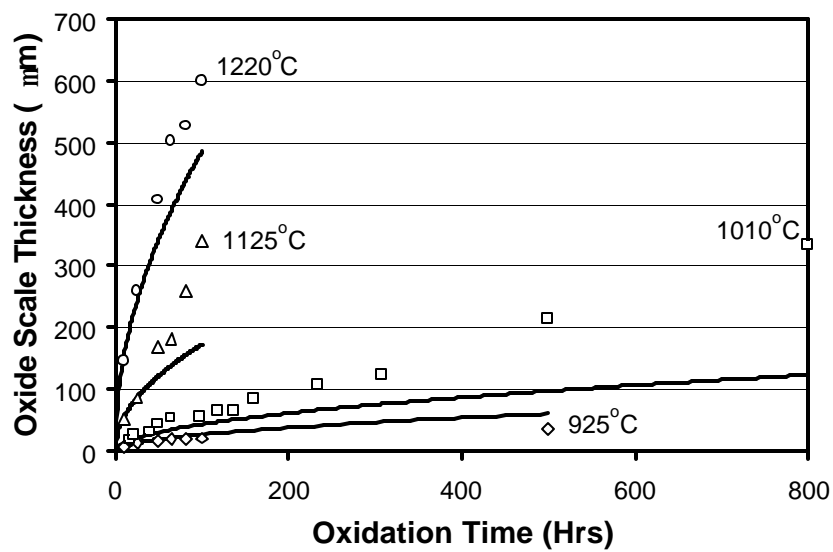
Figure 23: Oxidation data for S1500 from 925°C to 1220°C
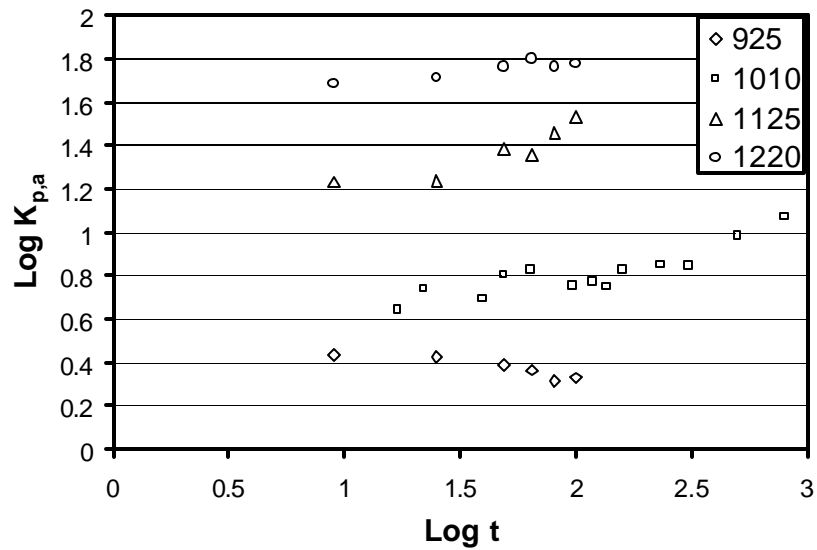
Figure 24: Log-log plot of $K_{p,a}$ vs. t for S1500 as per Nickel model
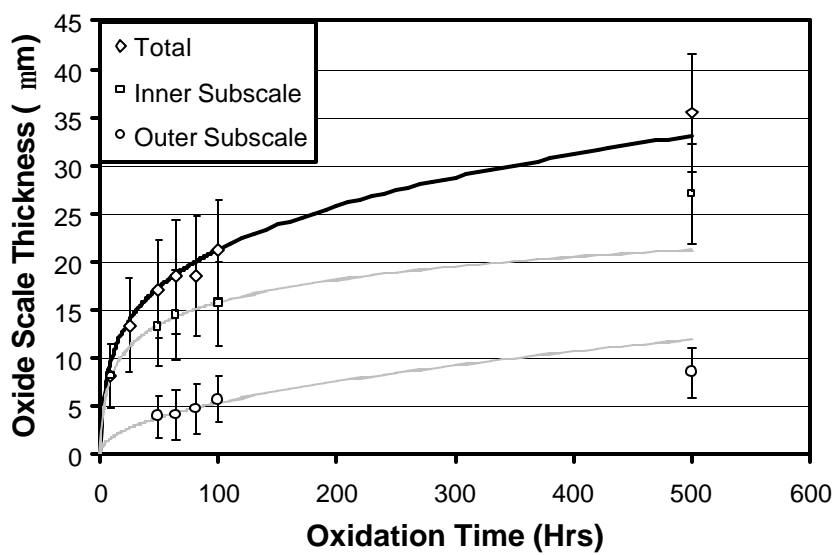
Figure 25: Growth of the oxide scale and subscales of S1500 at 925°C
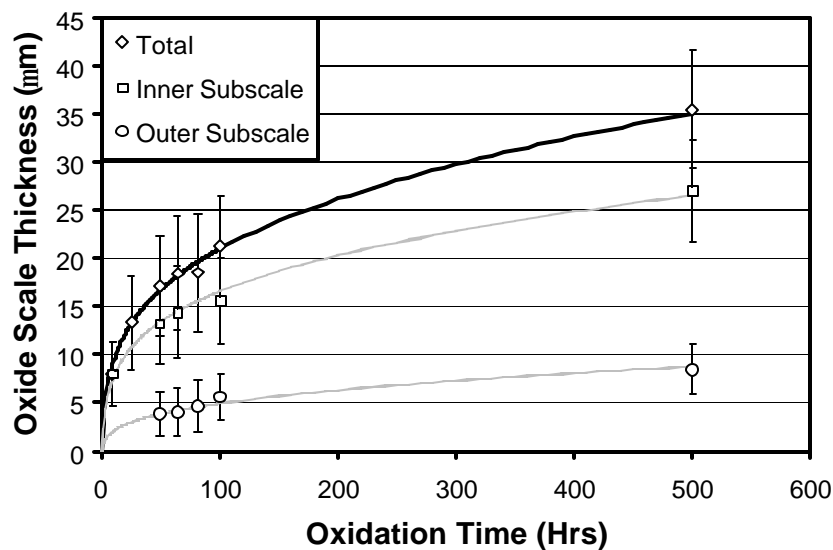
Figure 26: Growth of the oxide scale and subscales of S1500 at 925°C, with data fit to include 500 hours data
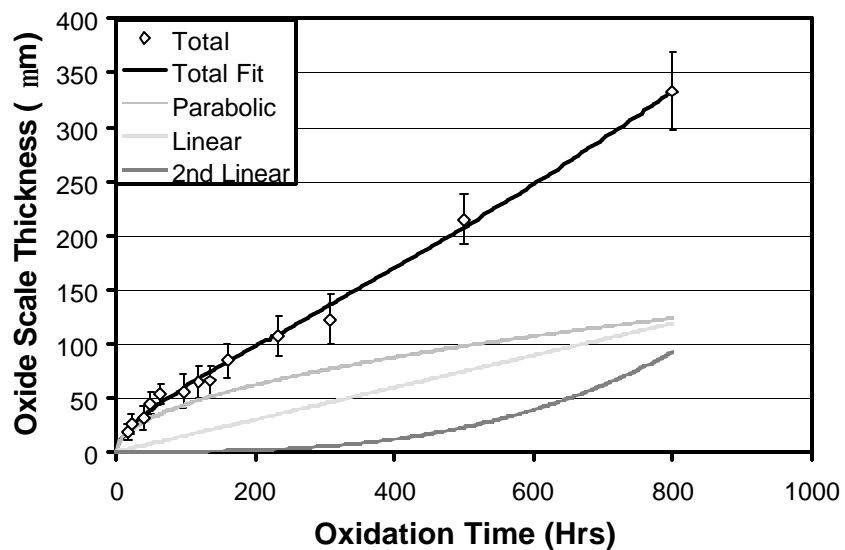
Figure 27: Growth of the oxide scale of S1500 at 1010°C
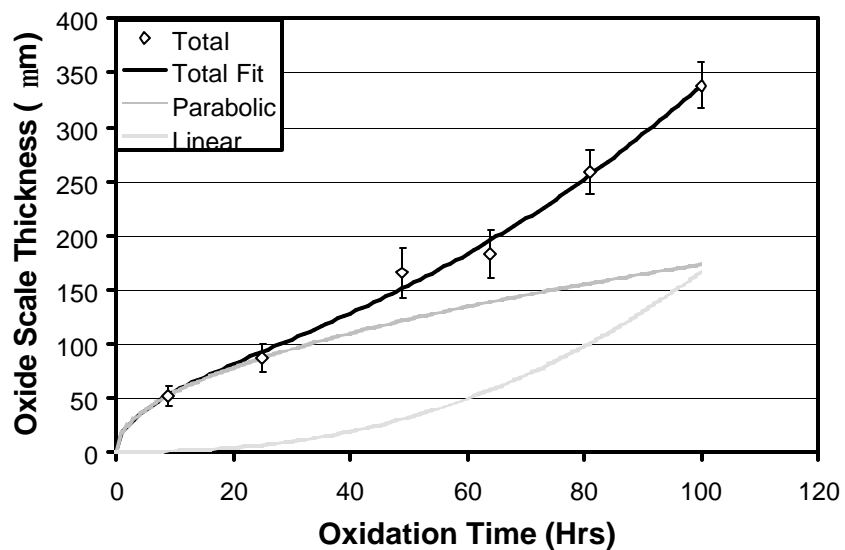
Figure 28: Growth of the oxide scale of S1500 at 1125°C
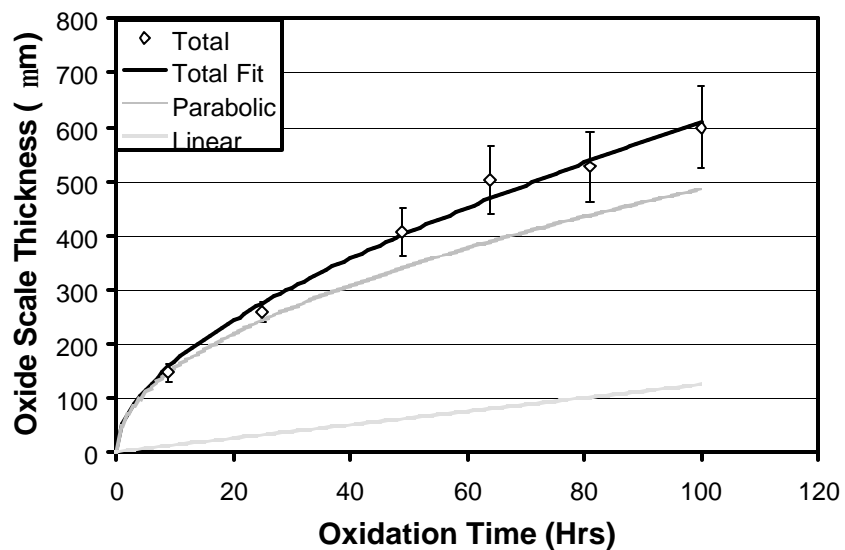
Figure 29: Growth of the oxide scale of S1500 at 1220°C
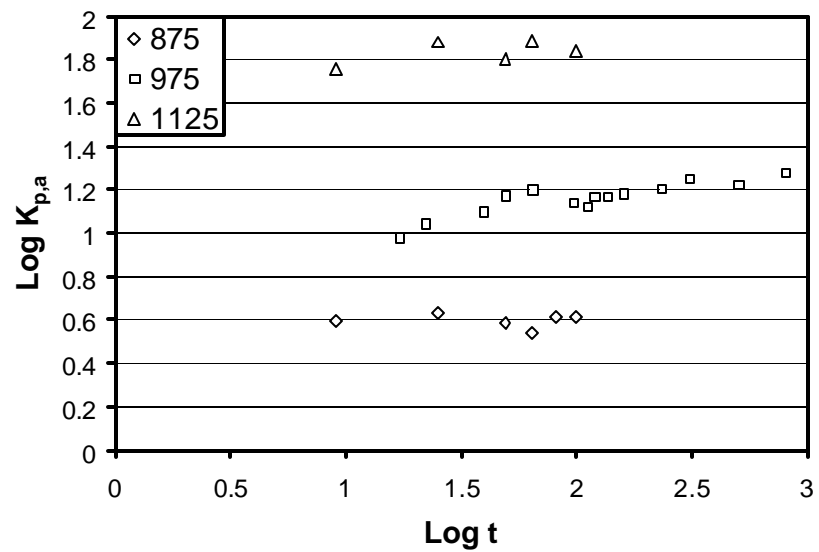
Figure 30: Log-log plot of $K_{p,a}$ vs. t for T1500 as per Nickel model
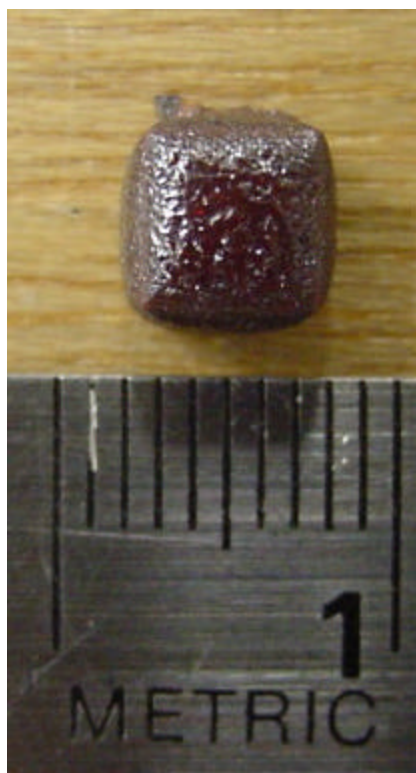
Figure 31: Picture of T1500 sample oxidized at 1220°C for 49 hours
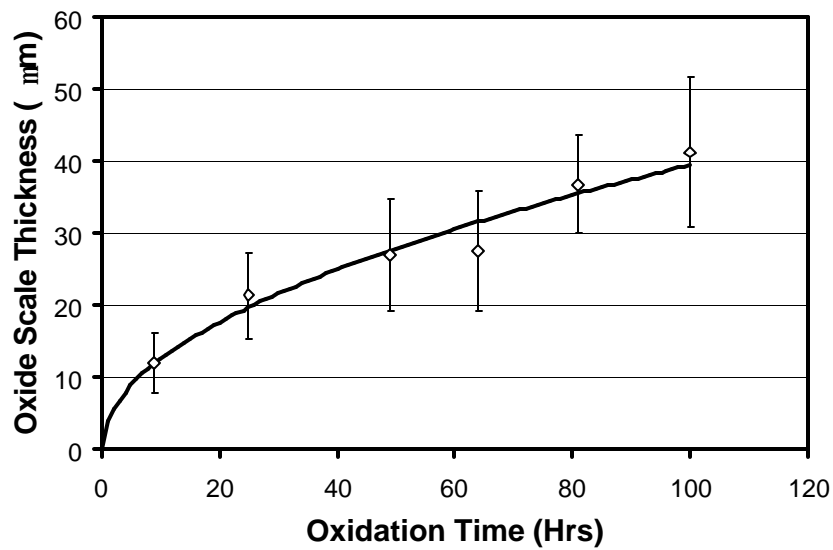
Figure 32: Growth of the oxide scale of T1500 at 875°C
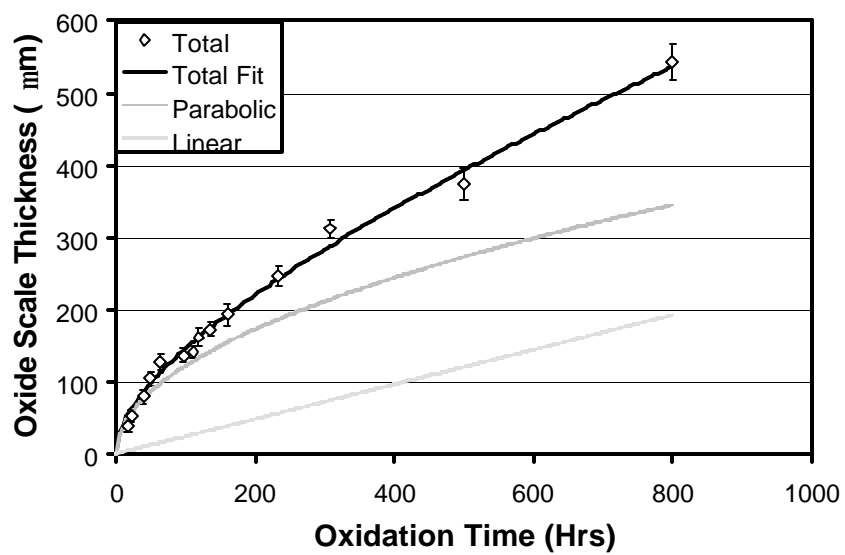
Figure 33: Growth of the oxide scale of T1500 at 975°C
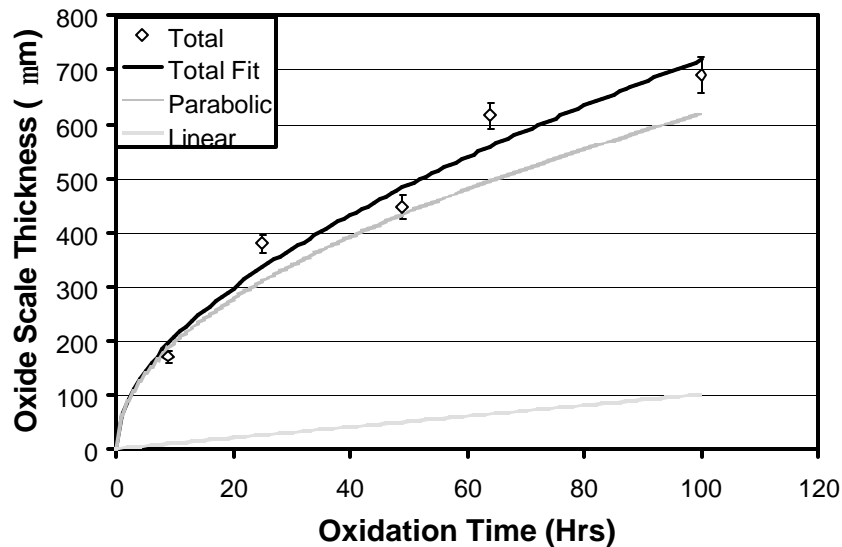
Figure 34: Growth of the oxide scale of T1500 at 1125°C
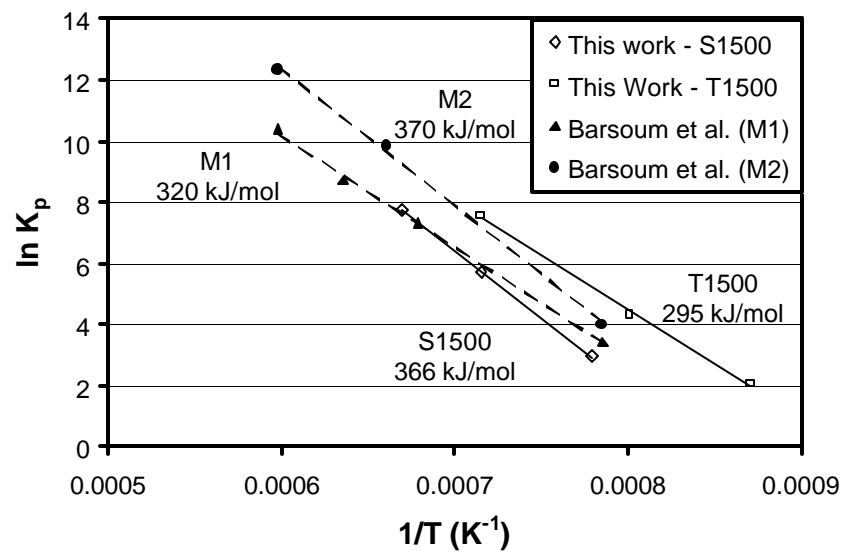
Figure 35: Arrhenian plots and activation energies for oxidation of S1500 and T1500 compared to data for pure Ti$_3$SiC$_2$[47]
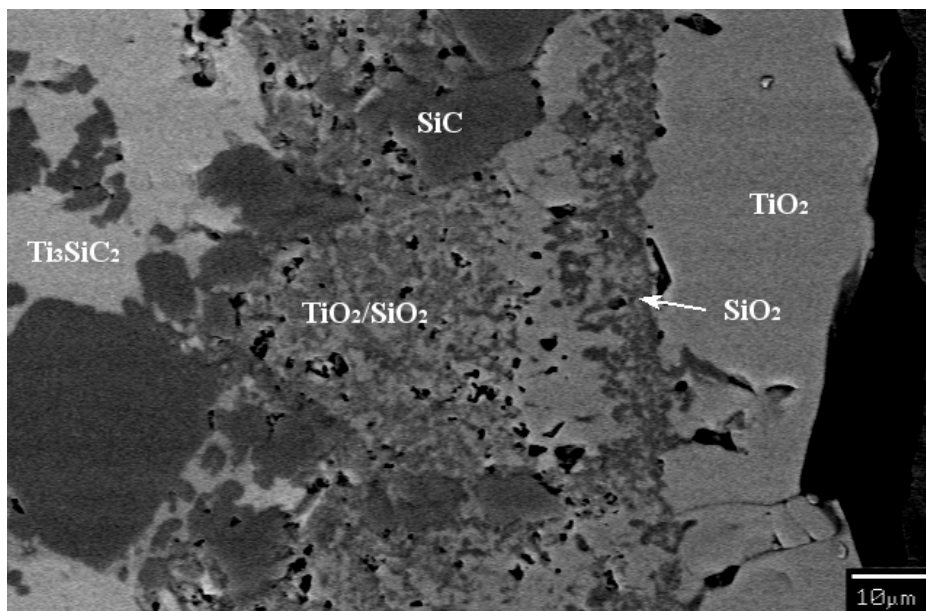
Figure 36: Backscattered SEM picture of S1500 oxidized at 1125°C for 25 hours
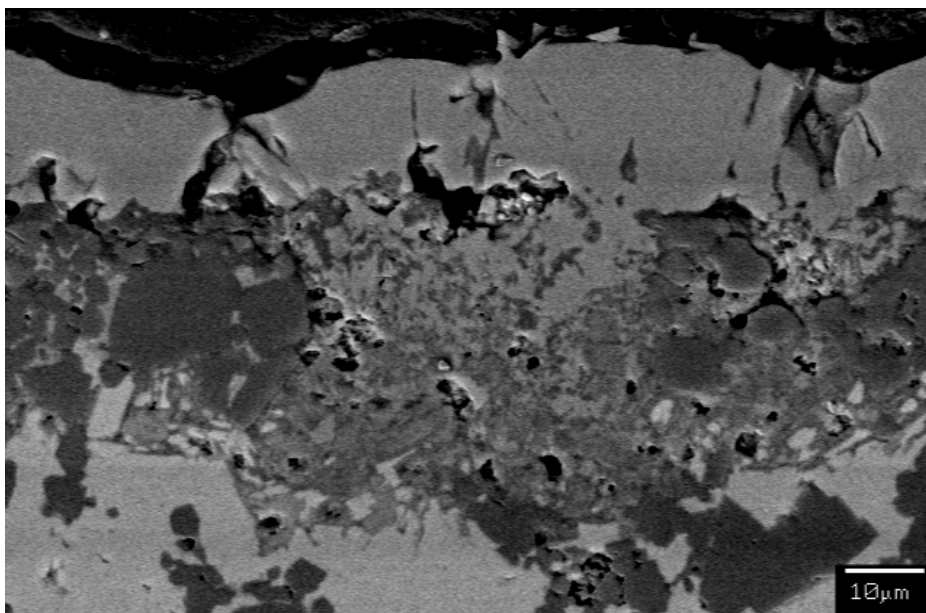
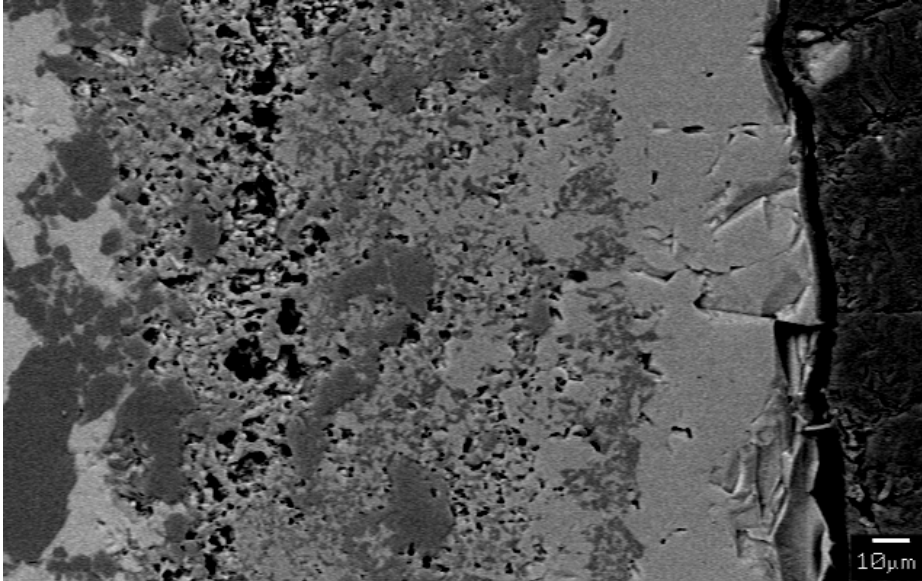**Figure 37: Backscattered SEM picture of S1500 oxidized at 1125°C for 9 hours**

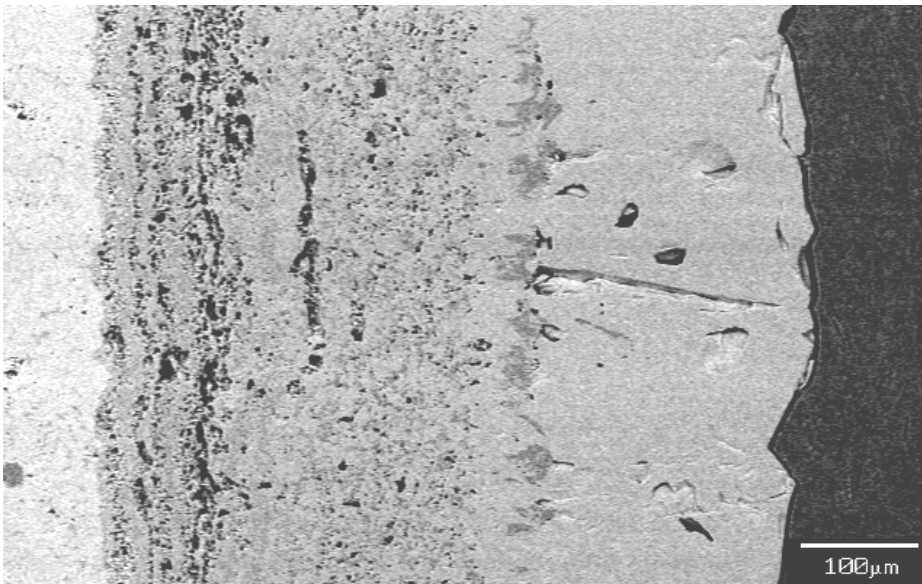**Figure 38: Backscattered SEM picture of S1500 oxidized at 1125°C for 64 hours**

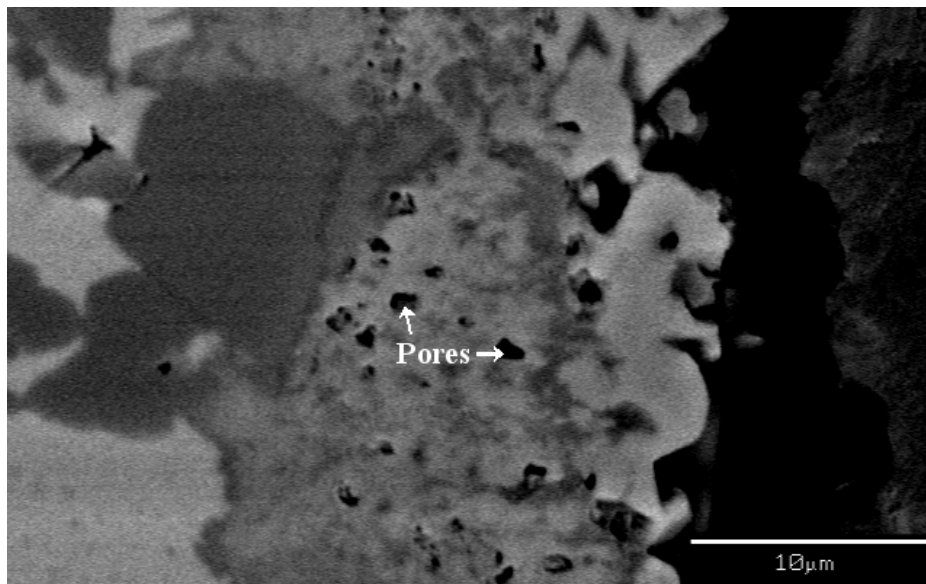**Figure 39: Backscattered SEM picture of T1500 oxidized at 1125°C for 64 hours**

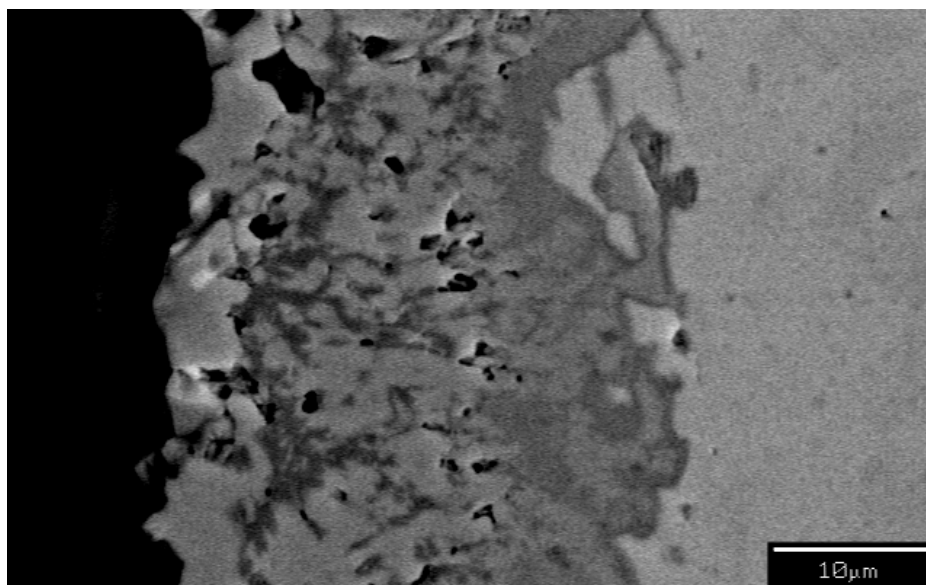**Figure 40: Backscattered SEM picture of S1500 oxidized at 925°C for 100 hours**

Figure 41: Backscattered SEM picture of T1500 oxidized at 875°C for 81 hours